nature biomedical engineering

Article

https://doi.org/10.1038/s41551-026-01677-9

STRAIGHT-IN Dual: a platform for dual single-copy integrations of DNA payloads and gene circuits into human induced pluripotent stem cells

Received: 15 December 2025

Accepted: 1 April 2026

Published online: 30 April 2026

Check for updates

Albert Blanch-Asensio[1,2,3], Deon S. Ploessl[3], Benjamin B. Johnson[1,2], Sara Cascione[1], Myrthe R. M. Berndsen[1,2], Nathan B. Wang[3], Valeria V. Orlova[1,2], Anna Alemany[1,2], Christine L. Mummery[1,2], Kate E. Galloway[3] ✉ & Richard P. Davis[1,2] ✉

Targeting DNA payloads into human induced pluripotent stem cells (hiPSCs) typically requires multiple inefficient steps, slowing the testing of gene circuits and cell-fate programmes. Here we show that STRAIGHT-IN Dual enables simultaneous, allele-specific, single-copy integration of two DNA constructs efficiently within 1 week. STRAIGHT-IN Dual leverages the STRAIGHT-IN platform for near-scarless payload integration, facilitating the recycling of components for further modifications. Using STRAIGHT-IN Dual, we investigate how promoter choice and gene syntax influence transgene silencing and how these design features affect reporter expression and forward programming of hiPSCs into neurons, motor neurons and endothelial cells. We also incorporate a grazoprevir-inducible synthetic gene switch that complements tetracycline-inducible control, providing tunable and temporally controlled expression of different transcription factors within the same cell. STRAIGHT-IN Dual generates homogeneous engineered hiPSC populations, accelerating synthetic biology design–build–test cycles in stem cells and enabling controlled comparisons of circuit performances.

Efficient, precise insertion of large DNA payloads into the mammalian genome remains a bottleneck for synthetic biology, disease modelling and cell-based therapies. Applications such as integrating reporters and biosensors, introducing disease-variant cassettes and programmable cell-fate circuits, and generating humanized mouse models all benefit from reliable genomic integration tools[1–7]. Recently, hybrid platforms combining genome editing technologies such as prime editing with site-specific recombinases (SSRs) have enabled insertion of DNA fragments up to 36 kb, offering a promising route for complex genome engineering[8–10]. However, genome engineering methods based on CRISPR–Cas9 can show variable efficiencies and require extensive clonal screening to identify correctly engineered lines.

SSR-based methods can address this limitation by enabling high-fidelity insertion of large payloads (>100 kb) into engineered landing pad (LP) cassettes[2,11–13]. In particular, the serine recombinase Bxb1 supports efficient, irreversible integration of large DNA constructs

[1]Department of Anatomy and Embryology, Leiden University Medical Center, Leiden, The Netherlands. [2]The Novo Nordisk Foundation Center for Stem Cell Medicine, reNEW, Leiden University Medical Center, Leiden, The Netherlands. [3]Department of Chemical Engineering, Massachusetts Institute of Technology, Cambridge, MA, USA. ✉e-mail: katiegal@mit.edu; r.p.davis@lumc.nl

into defined genomic sites[4,14,15]. However, most SSR-based platforms are restricted to single-copy integration at a single locus. While some platforms permit integration of two DNA payloads[16], few support precise, allele-specific insertion of multiple transgenes. Alternative methods, such as cassette exchange, which relies on two recombination sites[17], remain relatively inefficient.

We previously developed STRAIGHT-IN, a modular Bxb1-based system for single-copy transgene integration into hiPSCs[2]. Although we evaluated the recombinase ϕC31 for orthogonal integration of two donor plasmids, its low efficiency precluded practical use. More recently, engineered orthogonal Bxb1 *attP*/*attB* variants in which the central 'GT' dinucleotide is altered to 'GA' were shown to maintain high integration efficiency with minimal crossover between the recombination sequences[15,18], creating an opportunity for multi-payload integration using a single recombinase.

Here we develop STRAIGHT-IN Dual, an hiPSC acceptor line carrying two orthogonal Bxb1-compatible LPs. This design enables simultaneous, allele-specific integration of two DNA payloads into distinct alleles of the *CLYBL* locus, a genomically permissive site proposed as a safe harbour[19]. STRAIGHT-IN Dual also supports Cre- and Flp-mediated removal of auxiliary sequences (for example, selection markers and vector backbones), generating markerless, near-scarless integrations[2,11,20]. The resulting platform supports iterative genome engineering while controlling for locus-specific and neighbouring transgene effects.

Using STRAIGHT-IN Dual, we systematically tested how promoter choice and gene syntax (the relative order and orientation of genes) influence transgene expression and stability across pluripotent and differentiated cell states. We also combined multiplexed construct integration with Flow-Seq[21] to establish a scalable framework for high-throughput screening of genetic components. In addition, we used the dual-LP configuration to improve forward programming of hiPSCs into induced motor neurons (iMNs) by distributing transcription factors across the two LPs. Finally, we adapted a grazoprevir (GZV)-inducible synthetic zincfinger transcription regulator (synZiFTR) system[22] for hiPSCs and combined it with doxycycline (Dox)-inducible Tet-On control to enable precise, independent regulation of two genetic programmes in the same cell.

Together, STRAIGHT-IN Dual provides a robust and flexible platform for multi-transgene integration and inducible control in hiPSCs. These capabilities support applications ranging from high-throughput genetic screening to combinatorial circuit design and multi-lineage modelling.

Bxb1 mediates allele-specific integration of two DNA payloads in *CLYBL*

Building on our STRAIGHT-IN acceptor hiPSC line containing a single LP in one allele of *CLYBL* (LU99_CLYBL-bxb-v2)[23], we targeted the unedited *CLYBL* allele to generate a dual-LP acceptor line. The original LP contains a Bxb1-GT *attP* site for allele-specific targeting with GT donor plasmids, an excisable PGK promoter-driven EBFP2 (constitutively fluorescent blue fluorescent protein) fluorescent reporter and a selection cassette (*BleoR*) designed as a promoter trap owing to the lack of an ATG initiation codon and promoter sequence. The 5′ and 3′ ends of the LP are flanked by two heterospecific *loxP* and *lox257* sites, enabling Cre recombinase to excise the auxiliary sequences both upstream and downstream of the payload after integration (Fig. 1a).

Using TALENs, we targeted a second LP containing an orthogonal Bxb1-GA *attP* site into the unedited *CLYBL* allele (Fig. 1a). This LP also included the red fluorescent reporter mScarlet, a puromycin selection cassette (*PuroR*), and heterospecific *FRT*/*F3* sites for Flp recombinase-mediated excision. We characterized an mScarlet-expressing hiPSC clone (STRAIGHT-IN Dual) by genotyping PCR, ddPCR and Sanger sequencing, confirming single-copy targeting of the Bxb1-GA *attP* LP (GA allele) in the previously unedited *CLYBL* allele with intact recombination sites (Fig. 1b,c and Supplementary Fig. 1a). The hiPSC line also showed a normal karyotype and retained pluripotency and trilineage differentiation capacity (Supplementary Fig. 1b–f).

We next generated donor plasmids containing either Bxb1-GT or Bxb1-GA *attB* recombination sites (GT or GA donors). In the presence of Bxb1, GT donors integrate into the Bxb1-GT *attP* LP (GT allele) and GA donors into the Bxb1-GA *attP* LP (Fig. 1a), enabling allele-specific cargo integration. The donor plasmids were designed to activate the corresponding promoter-trap selection markers upon correct integration, conferring zeocin (GT; *BleoR*) or puromycin (GA; *PuroR*) resistance.

Before selection, integration frequencies were comparable for both alleles (GT, 1.09% ± 0.21; GA, 1.10% ± 0.02; Fig. 1d,e). Following antibiotic selection, edited populations containing either the GT or GA donor plasmids were enriched to 95.52% ± 1.87 (GT) and 99.06% ± 0.08 (GA) (Fig. 1d,e). Co-transfection of both donor plasmids together with a Bxb1 expression plasmid, followed by dual selection, resulted in >93.9% of hiPSCs containing both integrated payloads (Extended Data Fig. 1a,b).

To confirm allele specificity, we transfected either donor plasmid and applied the non-matching antibiotic selection. Incorrect integration of the GT donor into the GA allele would confer puromycin resistance, whereas incorrect integration of the GA donor into the GT allele would confer zeocin resistance (Fig. 1f). In both cases, mismatched selection resulted in no cell survival, confirming orthogonality (Fig. 1f).

We further validated this using fluorescent cargoes by cloning green and red fluorescent reporters (TurboGFP and mScarlet-I, respectively) into both donor plasmids (Fig. 1g). TurboGFP was tagged with a nuclear localization sequence (NLS) and mScarlet-I with an actin-targeting signal, enabling unambiguous visualization of each transgene within individual cells. Co-transfection of two fluorescent payloads targeting the same LP (either GT or GA allele) yielded cells expressing only one fluorophore, consistent with mutually exclusive integration. By contrast, co-transfection of TurboGFP-GT and mScarlet-I-GA donor plasmids produced dual-labelled hiPSCs (Fig. 1g). No integration was detected when the TurboGFP-GA donor was transfected into the parental CLYBL-bxb-v2 hiPSC line, which lacks the GA allele, further supporting allele specificity and excluding detectable off-target integration (Extended Data Fig. 1c). Finally, integrating the same reporter into both LPs increased the fluorescence signal ~2-fold, suggesting that both *CLYBL* alleles support comparable levels of transgene expression (Extended Data Fig. 1d).

Accelerating and simplifying the STRAIGHT-IN Dual protocol improves cell line generation

To streamline the generation of uniform, genetically modified hiPSCs, we optimized the STRAIGHT-IN integration process to improve efficiency, increase cell yield and shorten the time to downstream experiments (Fig. 2a). We hypothesized that the lower cytotoxicity and higher transgene expression typically observed with modRNA delivery compared with plasmid DNA in hiPSCs would improve integration outcomes. Indeed, transfection of Bxb1 modRNA resulted in an ~2-fold increase in integration efficiency (Extended Data Fig. 1e).

Next, we explored whether co-delivery of cytoprotective factors could improve post-transfection survival, as reported for CRISPR-based genome editing[24]. Co-transfection of p53 variant (p53DD) modRNA increased the proportion of hiPSCs with an integrated cargo by 12.4-fold compared with a control *mGreenLantern* modRNA (Extended Data Fig. 1f). We also evaluated four engineered Bxb1 variants with reported improvements in recombination activity[9,25], namely evoBxb1 (V74A), eeBxb1 (V74A + E229K + V375I), Bxb1-I87L and Bxb1-I87L + A369P + E434G. Among these, eeBxb1 delivered as modRNA and combined with p53DD modRNA significantly increased pre-selection integration efficiency from 2.75% to 9.12% at the GT allele,

https://doi.org/10.1038/s41551-026-01677-9

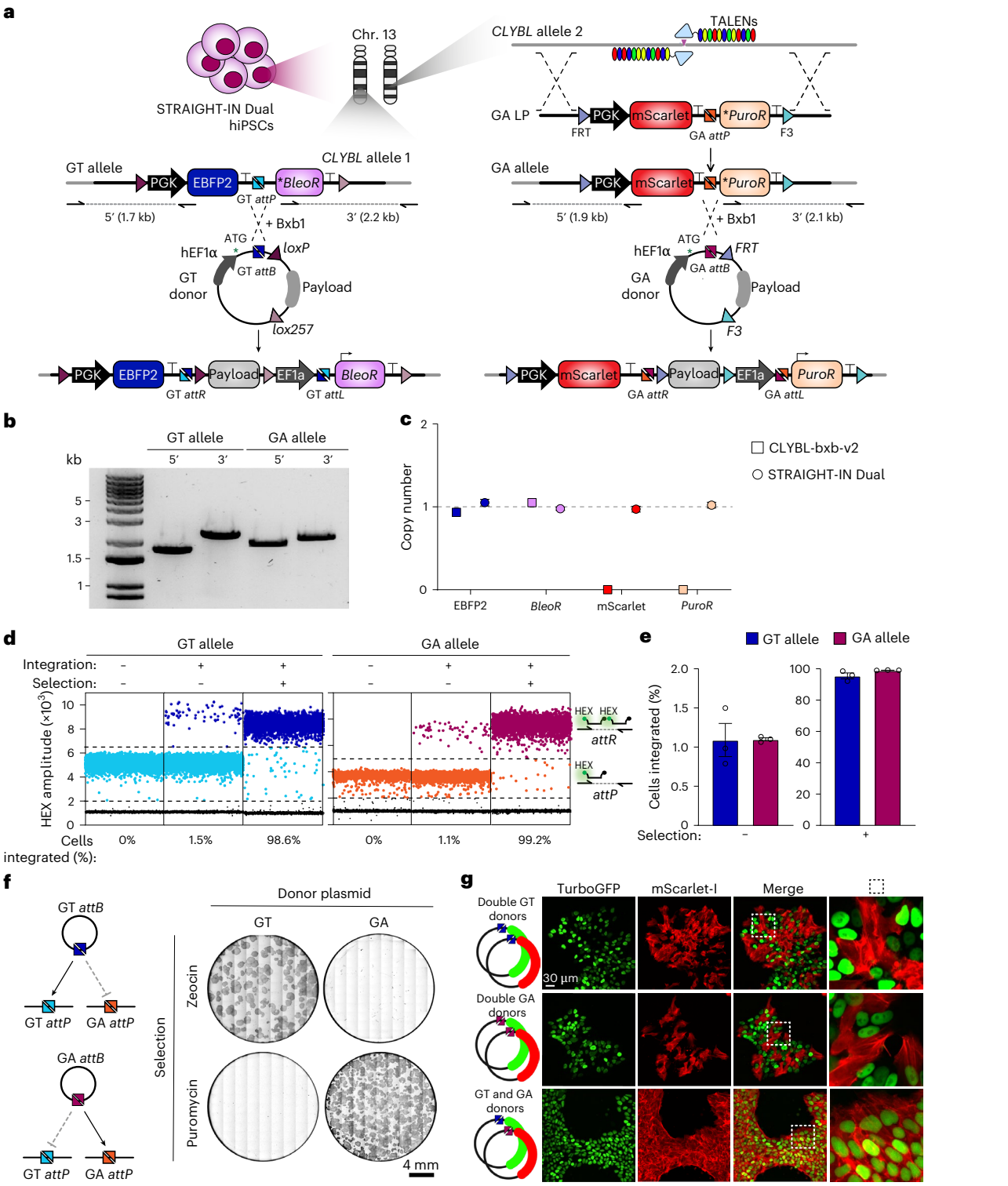

Fig. 1 | Allele-specific targeting of GT and GA donor plasmids in the STRAIGHT-IN Dual hiPSCs. a, Schematic of TALEN-mediated targeting of the GA-LP cassette into the second allele of the *CLYBL* locus and Bxb1 recombinase-mediated integration of GT and GA donor plasmids into their cognate LPs. Expression of the antibiotic resistance markers (*BleoR* and *PuroR*) is activated only upon correct donor plasmid integration, which supplies the missing initiation codon (*). Half arrows indicate junction PCR primer sites. 'Payload' indicates the location of the desired DNA cargo for targeting in both the donor plasmid and following genomic integration. 'T' denotes polyadenylation sequences. **b**, Junction PCR analysis confirming targeting of GT and GA alleles in the *CLYBL* locus. **c**, ddPCR validating single-copy genomic integration of each LP cassette. The CLYBL-bxb-v2 hiPSC line serves as a control. Symbols indicate the estimated copy number; error bars indicate the Poisson 95% confidence interval. Data are from a single engineered acceptor line measured once ($N = 1$). **d**, Representative ddPCR dot plots showing GT and GA donor plasmid integration before and after antibiotic selection. Dots represent droplets containing the indicated sequence (*attR* or *attP*), with percentages showing the calculated integration efficiencies. **e**, Mean integration efficiencies of GT and GA donor plasmids before (−) and after (+) antibiotic selection. $N = 3$ independent transfections; error bars, ±s.e.m. **f**, Schematic illustrating Bxb1-GT/GA recombination specificity (left) and alkaline phosphatase staining (right) confirming orthogonal payload integration at the GT and GA alleles. **g**, Fluorescence images showing allele-specific expression of TurboGFP (GT) and mScarlet-I (GA) following donor plasmid integration. Schematics in **a** (Chr. 13) and **g** created in BioRender; Blanch Asensio, A. https://biorender.com/yu8eiiq (2026).

and from 1.46% to 11.7% at the GA allele (Fig. 2b). Other *Bxb1* variants did not outperform wild-type *Bxb1*, although co-transfection of p53DD modRNA consistently improved integration efficiencies across experiments (Extended Data Fig. 1g).

On the basis of these optimization experiments, and to expedite enrichment with zeocin or puromycin, we used modRNA for all subsequent donor plasmid integrations. Because modRNA results in more rapid Bxb1 expression than plasmid delivery, antibiotic selection could begin 1 day after transfection. This reduced the time required to obtain uniform, payload-carrying hiPSCs to less than 1 week (Fig. 2c,d). Notably, inclusion of p53DD modRNA enabled recovery of hiPSC colonies with both GT and GA integrations after only 3 days of antibiotic selection (Fig. 2e and Extended Data Fig. 1h). ddPCR confirmed single-copy insertions of the GT and GA donor plasmids, with no evidence of random integration (Extended Data Fig. 1i).

After integration, Cre and Flp recombinases are used to excise auxiliary elements, leaving behind only the DNA payload and often improving transgene expression[2] (Fig. 2f). While plasmid-based recombinase expression can yield high excision rates with selection, it often results in few surviving clones and prolonged expansion times. To improve this, we explored plasmid-free strategies using either modRNA or recombinant protein delivery.

For the GT allele, delivery of TAT-Cre protein resulted in excision rates of 91.9% and 80.7% for the *loxP*- and *lox257*-flanked sequences, respectively. A second round of TAT-Cre increased this to 97.6% and 93.7% (Fig. 2g). For the GA allele, where TAT-Flp protein is unavailable, we used *Flp* modRNA. After one transfection, 61.5% and 54.8% of hiPSCs had excised the *FRT*- and *F3*-flanked sequences, respectively, increasing to 87.8% and 76.3% with a second transfection (Extended Data Fig. 1j, left). Co-delivery of *TAT-cre* and *Flp* modRNA resulted in 83.6% of hiPSCs excising all flanked auxiliary sequences after 2 transfection rounds (Extended Data Fig. 1j, right).

We hypothesized that coupling excision to selection might further enhance efficiency, potentially enabling complete removal of auxiliary elements after a single transfection. To test this, we integrated a donor plasmid into the GA allele, conferring puromycin resistance while leaving cells zeocin sensitive. Transfection of a modRNA encoding both *Flp* and *BleoR* (Flp-T2A-BleoR), followed by zeocin selection starting 1 day later, resulted in near-complete excision of both upstream and downstream auxiliary elements within 3 days with efficiencies of 99.3% and 97.2%, respectively (Fig. 2h). However, an equivalent strategy could not be replicated with Cre for donor plasmids integrated at the GT allele, as puromycin selection following Cre-T2A-PuroR or Cre-IRES-PuroR modRNA transfection failed to yield puromycin-resistant hiPSCs. Co-transfection of Cre and PuroR modRNAs resulted in limited excision enrichment, with efficiencies increasing only from 25.7% to 44.3% for *loxP*- and from 22.5% to 41.7% for *lox257*-flanked sequences (Extended Data Fig. 1k).

Finally, to further streamline the protocol, we performed donor plasmid integration and auxiliary element excision in the same well without passaging the cells. The hiPSCs were co-transfected with eeBxb1 and p53DD modRNA together with a GA donor plasmid encoding enhanced green fluorescent protein (eGFP), followed by puromycin selection on days 1–3 after transfection. On day 4, Flp-T2A-BleoR modRNA was transfected, and zeocin selection was applied from days 5 to 8 (Fig. 2i). Within 9 days, hiPSCs showed near-uniform eGFP expression and excision of auxiliary elements (Fig. 2j,k), demonstrating a rapid, one-well protocol for near-scarless single-copy genome integration with >98% efficiency.

Identifying promoter sequences supporting stable transgene expression in hiPSCs

Transgenes are essential tools for tracking cellular processes and modulating cell behaviour and identity[26]. However, in hiPSCs, genome-integrated transgenes are susceptible to transcriptional silencing, particularly during prolonged culture or upon differentiation. Promoter choice has a crucial role in determining both expression strength and susceptibility to silencing[27,28] (Fig. 3a). Although the CMV early enhancer/chicken β-actin (CAG) and human elongation factor 1-α (hEF1α) promoters are commonly used for constitutive transgene expression across diverse cell types[29], their comparative performance in hiPSCs remains poorly defined.

To directly compare promoter activity, we generated a dual-reporter hiPSC line in which divergently oriented CAG and hEF1α promoters drove expression of mRuby2 and mGreenLantern, respectively. While all puromycin-resistant hiPSC colonies showed uniform mRuby2 expression, only a subset expressed mGreenLantern despite confirmed integration of the hEF1α-driven cassette, indicating transcriptional silencing. This effect became more pronounced with passaging (Extended Data Fig. 2a).

To exclude reporter-specific effects and promoter interference, we replaced mGreenLantern with mStayGold, the brightest monomeric GFP reported so far[30], and integrated the two reporters into separate *CLYBL* alleles. Again, only the hEF1α-driven mStayGold was silenced (Extended Data Fig. 2b). Swapping promoter–reporter pairings confirmed this result, with CAG-driven mStayGold strongly expressed while hEF1α-driven mRuby2 was silenced (Extended Data Fig. 2c).

We next screened a panel of 11 promoters to identify sequences capable of driving low, medium or high levels of transgene expression. In addition to hEF1α and CAG, the panel included ubiquitous promoters (UbC, β-actin and PGK), viral promoters (CMV, RSV and SV40), truncated CAG variants (CBh and shortCAG) and a CpG-depleted hEF1α variant (CpG-free). We introduced promoters either separately or in a multiplexed format to demonstrate the feasibility of integrating plasmid libraries using STRAIGHT-IN. This also enabled direct comparison

Fig. 2 | Optimized STRAIGHT-IN protocol improved integration and excision efficiencies while reducing timelines. a, Schematic of the rapid integration procedure. **b**, Mean integration efficiencies of GT and GA donor plasmids using modRNA combinations of Bxb1, eeBxb1 and p53DD before selection. $N = 3$ independent transfections; error bars, ±s.e.m.; not significant (NS), $P > 0.05$; *$P \leq 0.05$; **$P \leq 0.01$; ***$P \leq 0.001$; ****$P \leq 0.0001$ (unpaired two-tailed t-test). Exact P values are 0.1493, 0.0008, 0.0050, 0.0034, 0.0026 and <0.0001, respectively. **c**, Overlay of fluorescence and phase-contrast images (left) and flow cytometry analysis (right) showing reporter expression following rapid integration of GT or GA donor plasmids encoding mRuby2 or eGFP, respectively. Dashed lines denote untransfected STRAIGHT-IN Dual acceptor hiPSCs. **d**, Mean integration efficiencies of GT and GA donor plasmids following antibiotic selection. $N = 3$ independent transfections; error bars, ±s.e.m. **e**, Schematic of the dual payload integration and selection procedure (left), and overlay of fluorescence and phase-contrast images (right) after co-delivery of GT and GA donor plasmids encoding mScarlet-I and eGFP, respectively. **f**, Schematic for excising selection cassettes and plasmid backbones using Cre or Flp recombinases. Dashed lines indicate the sequences excised, and half arrows indicate primer sites for ddPCR analysis. **g**, Mean percentages of hiPSCs with indicated flanking regions excised following 1 (#1) or 2 (#2) administrations of TAT-Cre protein, as determined by ddPCR. $N = 3$ independent transfections; error bars, ±s.e.m. **h**, Mean percentages of hiPSCs with indicated flanking regions excised following Flp-2TA-BleoR modRNA transfection, with (+) or without (−) zeocin selection, as determined by ddPCR. $N = 4$ independent transfections; error bars, ±s.e.m. **i**, Schematic of the complete rapid integration and excision workflow. **j**, Representative fluorescence and phase-contrast images, and flow cytometry analysis of hiPSCs transfected with a GA-eGFP donor plasmid on days 4 and 9 of the STRAIGHT-IN rapid integration and excision workflow. Dashed lines represent untransfected STRAIGHT-IN Dual acceptor hiPSCs. **k**, Mean percentage of hiPSCs with indicated flanking regions excised after Flp-2TA-BleoR modRNA transfection and zeocin selection, as determined by ddPCR. $N = 3$ independent transfections; error bars, ±s.e.m. Schematics in **a**, **b**, **e** and **g**–**i** created in BioRender; Blanch Asensio, A. https://biorender.com/z42p366 (2026).

https://doi.org/10.1038/s41551-026-01677-9

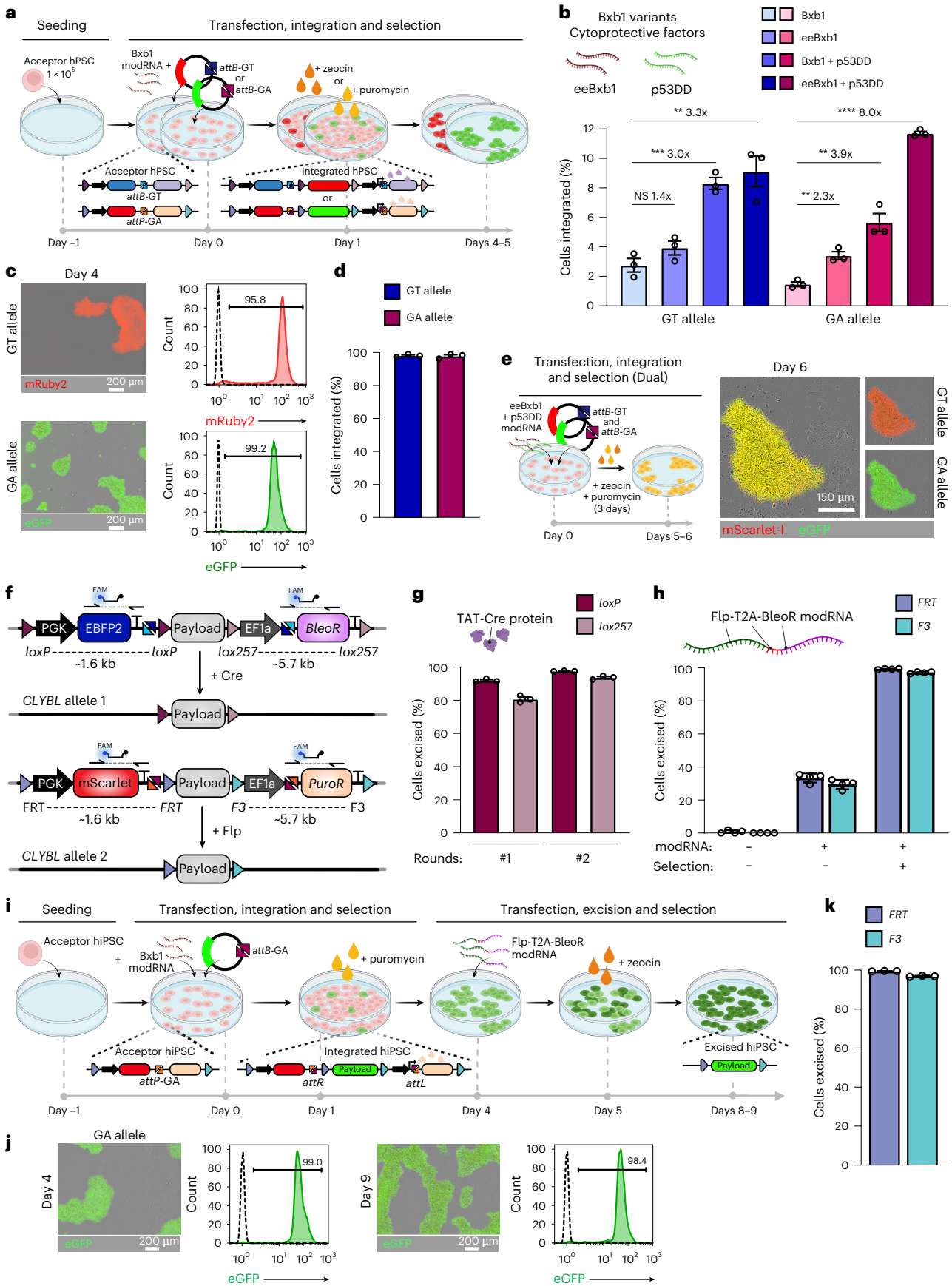

https://doi.org/10.1038/s41551-026-01677-9

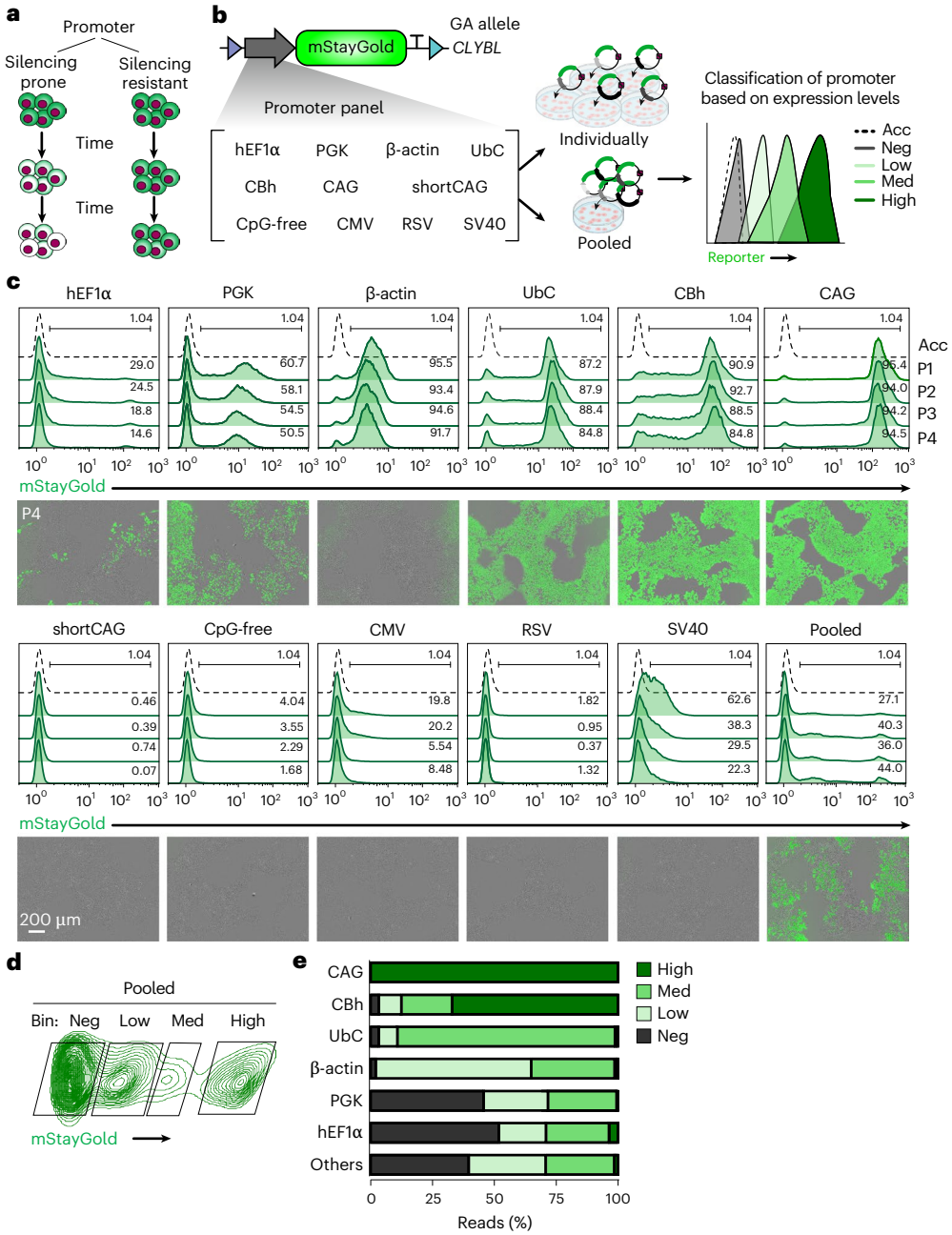

Fig. 3 | Evaluation of transgene silencing using STRAIGHT-IN. a, Conceptual schematic illustrating transgene silencing over time following genomic integration. **b**, Schematic of the panel of 11 different promoters, each driving expression of an mStayGold reporter integrated into the *CLYBL* locus. Donor plasmids were delivered either individually or as a pooled library to identify promoter sequences supporting high, medium and low transgene expression levels. **c**, Representative flow cytometry analysis (top), and overlaid fluorescence and phase-contrast images (bottom) over 4 passages of mStayGold expression in hiPSCs following individual promoter integration. Dashed lines indicate untransfected STRAIGHT-IN Dual acceptor hiPSCs. **d**, Flow cytometry analysis of the pooled integration approach, with the bulk population sorted into four mStayGold expression clusters: negative (neg), low, medium (med), and high. **e**, Bar graph showing the distribution of sequencing reads for the indicated promoter sequences mapping to each of the four expression clusters. Schematic in **b** created in BioRender; Blanch Asensio, A. https://biorender.com/iuybmqy (2026).

of pooled versus individual outcomes (Fig. 3b). While all promoters produced detectable mStayGold expression 24 h after transfection, their expression profiles diverged markedly following single-copy integration at the *CLYBL* locus, indicating potential context-dependent differences between episomal and integrated transgene expression (Extended Data Fig. 3a,b).

Among the candidates tested, full-length CAG consistently supported strongest mStayGold expression, followed by its truncated derivative CBh. UbC and β-actin promoter sequences produced intermediate and low expression levels, respectively, suggesting utility in applications requiring tighter control. By contrast, the remaining promoters (including hEF1α, CMV and CpG-free) either failed to produce homogeneous mStayGold expression or were rapidly silenced upon passaging (Fig. 3c). Longitudinal monitoring over ten passages showed sustained mStayGold expression from CAG and UbC promoters, while with hEF1α it remained silenced in most cells (Extended Data Fig. 3c).

We next evaluated promoter behaviour in a pooled context. All 11 promoter constructs were detected in the bulk population by next-generation sequencing (Extended Data Fig. 3d). Cells were binned into four mStayGold-based expression clusters (negative, low, medium

and high), and promoter sequences within each sorted cluster were mapped (Fig. 3d,e and Extended Data Fig. 3e). The expression patterns closely matched those from individually integrated lines: CAG and CBh were enriched in the high-expression cluster; UbC in the intermediate cluster; β-actin in the low-expression cluster; and hEF1α, PGK and the remaining promoters predominantly in the negative cluster.

To assess whether these results were locus dependent, we integrated 6 promoter constructs (hEF1α, CAG, UbC, CBh, β-actin and PGK) into an hiPSC line containing an LP at the adeno-associated virus integration site 1 (*AAVS1*) locus[23] (Supplementary Fig. 2a). As observed at the *CLYBL* locus, CAG again drove strong and stable transgene expression across multiple passages at *AAVS1*, whereas hEF1α- and PGK-containing constructs underwent silencing (Supplementary Fig. 2b). Notably, UbC, CBh and β-actin showed greater variability in both silencing and expression levels between the two loci, indicating that promoter and locus jointly influence transgene expression.

These findings guided further optimization of the STRAIGHT-IN donor plasmids. Because CAG consistently supported strong and stable transgene expression, whereas hEF1α was more prone to silencing, we designed the GT and GA donor plasmids to place the CAG promoter upstream of the transgene cloning site (Supplementary Fig. 3a). In addition, because the original GA donor plasmid relied on hEF1α to drive *PuroR* expression in the LP, we hypothesized that this could limit recovery of puromycin-resistant colonies. We therefore replaced hEF1α with CAG, UbC or CBh (Supplementary Fig. 3b). Following puromycin selection, colony numbers increased by 1.45-, 2.29- and 3.84-fold, respectively, indicating that weak hEF1α activity was impairing selection efficiency (Supplementary Fig. 3c).

Gene syntax influences induction efficiency in the Tet-On 3G system in hiPSCs

Beyond promoter selection, gene syntax, which is the relative order and orientation of transcriptional units, can influence the expression of adjacent genes[31–33]. While placing different components of gene circuits at separate genomic loci may reduce unwanted interactions, this approach also requires additional genomic integrations. To systematically compare how multi-component gene circuits perform, we used STRAIGHT-IN Dual to identify design principles for the Tet-On 3G system, examining trade-offs between co-localized (*cis*) and dual-locus (*trans*) configurations.

We first constructed a *trans* design with the transcriptional units integrated into separate *CLYBL* alleles (Fig. 4a). The inducible mScarlet reporter was driven by a tetracycline response element (TRE) containing seven tetracycline operator (*TetO*) repeats. On the basis of our observation that the CAG promoter resists silencing in hiPSCs, we used CAG to drive transactivator gene (rtTA) expression in a bicistronic cassette that also expressed a nuclear-localized blue fluorescent reporter (mTagBFP2-NLS) as a proxy readout for rtTA levels.

We also generated *cis* designs, in which both the constitutive (rtTA-T2A-mTagBFP2-NLS) and inducible (TRE-mScarlet) transcriptional units were integrated into the same allele. This allowed us to test how gene syntax affects induction. We created four syntaxes: convergent, divergent, downstream tandem and upstream tandem (Fig. 4a). Because the unexcised GA allele retains auxiliary sequences, including mScarlet (resulting in two copies of mScarlet in these lines), we quantified mTagBFP2 and mScarlet expression both before (Extended Data Fig. 4) and after auxiliary sequence excision (Fig. 4).

In the *trans* configuration, induced mScarlet expression was weak, whereas several *cis* designs showed robust induction (Fig. 4b), suggesting that spatial proximity between the constitutive and inducible units improves Tet-On 3G induction in hiPSCs. Notably, mTagBFP2 expression levels were unchanged in the *trans* configuration, indicating that reduced induction was unlikely due to differences in rtTA expression (Fig. 4c,d).

Before induction, we observed clear bimodality in mTagBFP2 expression for the convergent syntax, which was most pronounced in unexcised cells (Extended Data Fig. 4c), and consistent with biophysical models of transcription[32]. By contrast, the other syntaxes exhibited unimodal mTagBFP2 expression, which remained stable upon induction with 1 μM doxycycline (Extended Data Fig. 4c). In unexcised cells, induction resulted in slight repression of mTagBFP2 across all syntaxes (Extended Data Fig. 4d), with syntax-specific differences in mTagBFP2 expression becoming evident after excision (Fig. 4c,d). Most notably, the downstream tandem syntax exhibited an approximately fivefold reduction in mTagBFP2 expression, while the convergent syntax showed no change. The divergent and upstream tandem syntaxes showed increased mTagBFP2 expression, in line with biophysical model predictions (Fig. 4c,d).

Upon induction with 1 μM doxycycline, notable syntax-specific differences also emerged in mScarlet expression. Although these differences became more pronounced after excision (Fig. 4b–d), similar trends were observed before excision (Extended Data Fig. 4e,f). The divergent and downstream tandem syntaxes showed strong mScarlet induction, whereas the convergent and upstream tandem syntaxes exhibited poorer induction, characterized by weak, bimodal or broad expression distributions. Excision substantially improved induction for the convergent syntax, possibly by increasing rtTA levels (as indicated by mTagBFP2), but did not improve induction for the upstream tandem syntax (Fig. 4c,d).

Given the robust mScarlet induction observed in the downstream tandem *cis* design, we next tested its performance in three-dimensional (3D) stem cell-derived cardiac organoids (cardioids), which provide a more complex cellular environment for disease modelling and developmental studies. mScarlet expression could be modestly tuned by varying doxycycline concentration (Fig. 4e), or altering the duration of exposure, with longer inductions leading to higher expression (Fig. 4f). mScarlet expression could be induced in later-stage cardioids when doxycycline was added from day 7, indicating that transgene expression can be dynamically controlled in complex 3D systems.

Fig. 4 | Gene syntax modulates performance of the Tet-On 3G system in hiPSCs. a, Schematic overview of a *trans*-acting design and the four possible all-in-one Tet-On 3G syntaxes in *cis*-acting design, defined by the relative orientation and order of the constitutive (rtTA-T2A-mTagBFP2) and doxycycline-inducible (TRE-mScarlet) transcriptional units. Arrows indicate transcriptional direction. **b**, Representative fluorescence/phase-contrast images (left) of hiPSCs carrying the integrated constructs shown in **a**, cultured in the absence (−) or presence (+) of doxycycline for 3 days. The schematic (right) summarizes relative mScarlet expression across syntaxes. Conv, convergent; Div, divergent; D-tand, downstream tandem; U-tand, upstream tandem. **c**, Flow cytometry analysis of mScarlet and mTagBFP2 expression in hiPSCs carrying each of the integrated constructs, in the absence (dashed line) or presence (red/blue) of doxycycline for 3 days. Values indicate fold change, which is based on geometric mean fluorescence intensity (G-mean). **d**, Quantification of G-mean values for mScarlet and mTagBFP2 expression in the absence (grey) or presence (red/blue) of doxycycline for 3 days. $N = 3$ biological replicates; mean ± s.e.m.; NS, $P > 0.05$; $^{****}P \leq 0.0001$ (one-way ANOVA). All exact P values are <0.0001. **e**, Dose–response of doxycycline-induced mScarlet expression in hiPSCs harbouring the downstream tandem construct. Representative fluorescence/phase-contrast images (top) and flow cytometry analysis with values indicating fold changes based on the G-mean (bottom). **f**, Inducible mScarlet expression in cardioids carrying the downstream tandem construct. Schematic of the induction protocols (top). Flow cytometry analysis showing mScarlet expression in the absence (dashed line) or presence (red) of doxycycline for the indicated periods (bottom left). Fold change values (x) are based on the G-mean values relative to untreated cardioids. Representative fluorescence/phase-contrast images at different time points for the same indicated periods of doxycycline induction (bottom right). D, day. Schematic in **f** created in BioRender; Blanch Asensio, A. https://biorender.com/y38m260 (2026).

https://doi.org/10.1038/s41551-026-01677-9

Dual payload inducible system enables forward programming of hiPSCs into iNs and iMNs

Forward programming of hiPSCs into specific cell types is typically achieved by overexpressing lineage-defining transcription factors. However, suboptimal gene syntax may impair transcription factor expression and thereby inhibit cell-fate conversion (Fig. 5a). Given the striking differences that we observed between the two tandem orientations (Fig. 4d), we investigated whether gene syntax also influences forward programming outcomes when overexpressing *NGN2*, a pioneer transcription factor for neurons[34]. To

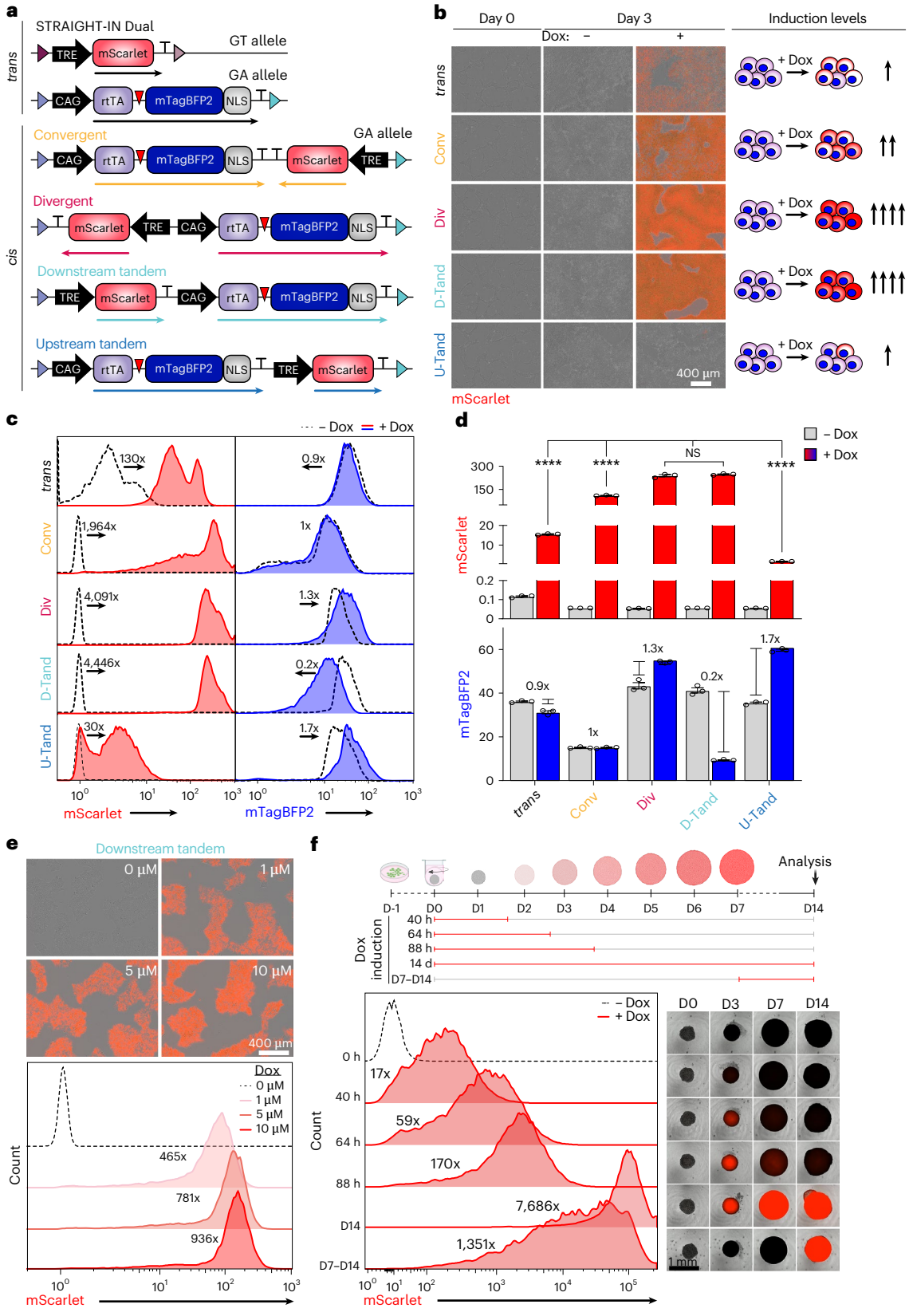

evaluate this, we constructed Tet-On 3G all-in-one systems to regulate NGN2 expression.

To enable rapid cloning of *NGN2* and other genes of interest into the STRAIGHT-IN LPs, we developed a modular set of tandem and divergent Tet-On 3G donor plasmids (Supplementary Fig. 4a). These vectors included a constitutive nuclear BFP reporter for visualization and a LacZ cassette to facilitate blue/white screening of bacterial colonies containing the cloned inserts. After assembly, >85% of white colonies carried the correct cargo (Supplementary Fig. 4b,c). This streamlined workflow allowed rapid generation of donor plasmids containing diverse inducible cargoes and, using the rapid integration protocol, establishment (within 1 week) of hiPSC lines that uniformly expressed the nuclear mTagBFP2 reporter (Supplementary Fig. 4d,e).

Induction of *NGN2* from the downstream tandem syntax led to generation of TUJ1$^+$MAP2$^+$ hiPSC-derived induced neurons (iNs) within 7 days (Fig. 5b and Extended Data Fig. 5a). By contrast, the upstream tandem configuration produced very few iNs (Fig. 5c), consistent with its weaker expression profile observed earlier (Fig. 4c,d). qPCR confirmed reduced induction of *NGN2* and other neuronal genes in the upstream tandem syntax, while pluripotency-associated genes were downregulated in the downstream tandem orientation following doxycycline induction (Fig. 5d).

To demonstrate the utility of STRAIGHT-IN Dual for co-expressing multiple transgenes, we integrated *NGN2* and a genetically encoded calcium indicator (jRCaMP1b) into separate *CLYBL* alleles using two TRE-controlled donor plasmids (Extended Data Fig. 5b). With doxycycline as a single inducer, this configuration resulted in rapid and robust forward programming of hiPSCs into iNs while simultaneously allowing monitoring of calcium signals (Extended Data Fig. 5c–e), illustrating how the Dual system can couple lineage conversion with real-time functional readouts.

We next investigated whether distributing the transcription factors required for motor neuron (iMN) specification (*NGN2*, *ISL1* and *LHX3*) across both LPs would improve the homogeneity of forward programming outcomes. Specifically, we compared a dual-cassette configuration in which *NGN2* and the *ISL1–LHX3* cassette were integrated separately (GT-NGN2 + GA-ISL1-LHX3; GT-N + GA-IL) with a single-cassette configuration in which all three factors were encoded in tandem within a single LP (GT-NGN2-ISL1-LHX3; GT-NIL; Fig. 5e). The single-cassette GT-NIL configuration led to a high proportion of proliferative, non-neuronal cells that rapidly overtook the culture (Extended Data Fig. 5f). By contrast, the dual-cassette strategy resulted in improved neuronal differentiation, yielding a purer population of iMNs (Extended Data Fig. 5f). Although in the single-allele approach, the non-neuronal cells were selectively eliminated by treatment with 5-ethynyl-2′-deoxyuridine (EdU), this step was not required for the dual-cassette design (Extended Data Fig. 5g,h).

After 10 days of differentiation, live-cell imaging with Hoechst and propidium iodide showed increased cell death in EdU-treated single-cassette cultures, consistent with the higher proportion of non-neuronal, EdU-sensitive cells (Extended Data Fig. 6a–d). Calcein AM staining and image quantification further showed that cells derived from the dual-cassette configuration were significantly larger, exhibited increased neurite branching and had longer dendrites (Extended Data Fig. 6a–d). qPCR confirmed that expression of *NGN2*, *ISL1* and *LHX3* was lower in the single-cassette configuration, while the dual-cassette cultures showed robust upregulation of motor neuron markers, including *HB9*, *CHAT* and *SLC18A3* (also known as *VAChT*), compared with *NGN2* alone (Extended Data Fig. 6e).

To evaluate the effects of copy number, allele configuration (*cis* versus *trans*) and transcript architecture, we generated three additional lines. To separate the effect of the tricistronic cassette while maintaining expression from a single allele, we expressed the transcription factors either as three separate inducible transcription units in a downstream tandem orientation (GA-N + I + L D-Tand), or as two units in a divergent syntax, with one encoding *NGN2* and the other carrying a bicistronic *ISL1–LHX3* cassette (GA-N + IL Div; Extended Data Fig. 7a,b). To test whether expression from the tricistronic NIL cassette could be increased, we introduced a second identical copy into the GA allele of the GT-NIL line (GT-NIL + GA-NIL; Fig. 5e). Dual integration resulted in an ~2-fold increase in mTagBFP2 expression (Fig. 5f), and after 3 days of doxycycline induction, this line exhibited the highest levels of all three transcription factors among the six lines analysed (Extended Data Fig. 7c).

By day 10 of differentiation, morphology and qPCR analysis indicated more robust motor neuron differentiation in the two dual-allele lines (GT-N + GA-IL and GT-NIL + GA-NIL), consistent with their increased transcription factor expression (Fig. 5g and Extended Data Fig. 7d,e). Immunofluorescence staining for HB9 further confirmed motor neuron identity (Fig. 5h and Extended Data Fig. 7f). Quantification of HB9$^+$ nuclei relative to total DAPI$^+$ nuclei showed that >85% of cells in the GT-N + GA-IL line were HB9$^+$ at day 10, whereas ~40% of cells were HB9$^+$ in the dual GT-NIL + GA-NIL line and <20% in the remaining lines (Fig. 5i and Extended Data Fig. 7g). Altogether, these data suggest that the single-transcript design may impede effective differentiation by limiting transcription factor expression. While increasing copy number improved both expression and differentiation, it did not achieve an efficiency similar to the split-allele GT-N + GA-IL hiPSC line.

Rapid generation of iECs and promoter activity profiling in differentiated lineages using STRAIGHT-IN Dual

To further demonstrate the versatility and efficiency of our all-in-one Tet-On 3G downstream-tandem vector system for generating inducible hiPSC lines, we cloned and overexpressed *ETV2*, a pioneer transcription factor that directs endothelial lineage specification (Extended Data Fig. 8a). Upon doxycycline induction, cells rapidly acquired an endothelial-like morphology and, by day 4, expressed key markers of endothelial identity, including CD31, ZO-1 and CD144 (Extended Data Fig. 8b–d).

Fig. 5 | Doxycycline-inducible expression of multiple transcription factors using STRAIGHT-IN Dual. a, Schematic of a forward programming strategy to generate specific cell types by inducible overexpression of transcription factors (TFs). **b**, Schematic of a downstream tandem all-in-one doxycycline-inducible *NGN2* cassette (top). Phase-contrast and immunofluorescence images (TUJ1, magenta; DNA, cyan) of cells at indicated days treated with (+) or without (−) doxycycline (bottom). **c**, Schematic of an upstream tandem all-in-one doxycycline-inducible *NGN2* cassette (top), with corresponding images to those shown in **b** (bottom). **d**, Expression analysis of pluripotency and neuronal marker genes in untransfected hiPSCs and cells containing inducible *NGN2* cassettes from **b** or **c**, treated with (+) or without (−) doxycycline for 7 days. Values are normalized to *RPL37A* and $\log_{10}$-transformed. $N = 3$ independent differentiations. **e**, Schematic of representative single- and dual-cassette configurations tested for forward programming hiPSCs to iMNs. **f**, Flow cytometry analysis of mTagBFP2 expression in hiPSC lines with the indicated cassettes integrated in the GT or GA alleles. Dashed line represents untransfected STRAIGHT-IN Dual acceptor hiPSCs, with values indicating G-mean fold change relative to the untransfected parental cell line. **g**, Gene expression analysis of inducible transcription factors and motor neuron markers in cells containing the indicated single- or dual-cassette configurations and cultured with doxycycline for 10 days. Values are normalized to *RPL37A* and shown relative to uninduced conditions ($\log_{10}$-transformed). $N = 3$ independent differentiations. **h**, Immunofluorescence images (MAP2, magenta; HB9, yellow; DNA, cyan) of the indicated cell lines treated with doxycycline for 10 days. **i**, Box-and-whisker plots showing the percentage of HB9$^+$ nuclei relative to DAPI$^+$ nuclei from images acquired as in **h**. The centre line indicates the median (50th percentile). The lower and upper bounds of the box indicate the 25th and 75th percentiles (interquartile range), and whiskers extend to the minimum and maximum values. For each condition, 2–3 images were analysed per differentiation across 3 independent differentiations.

https://doi.org/10.1038/s41551-026-01677-9

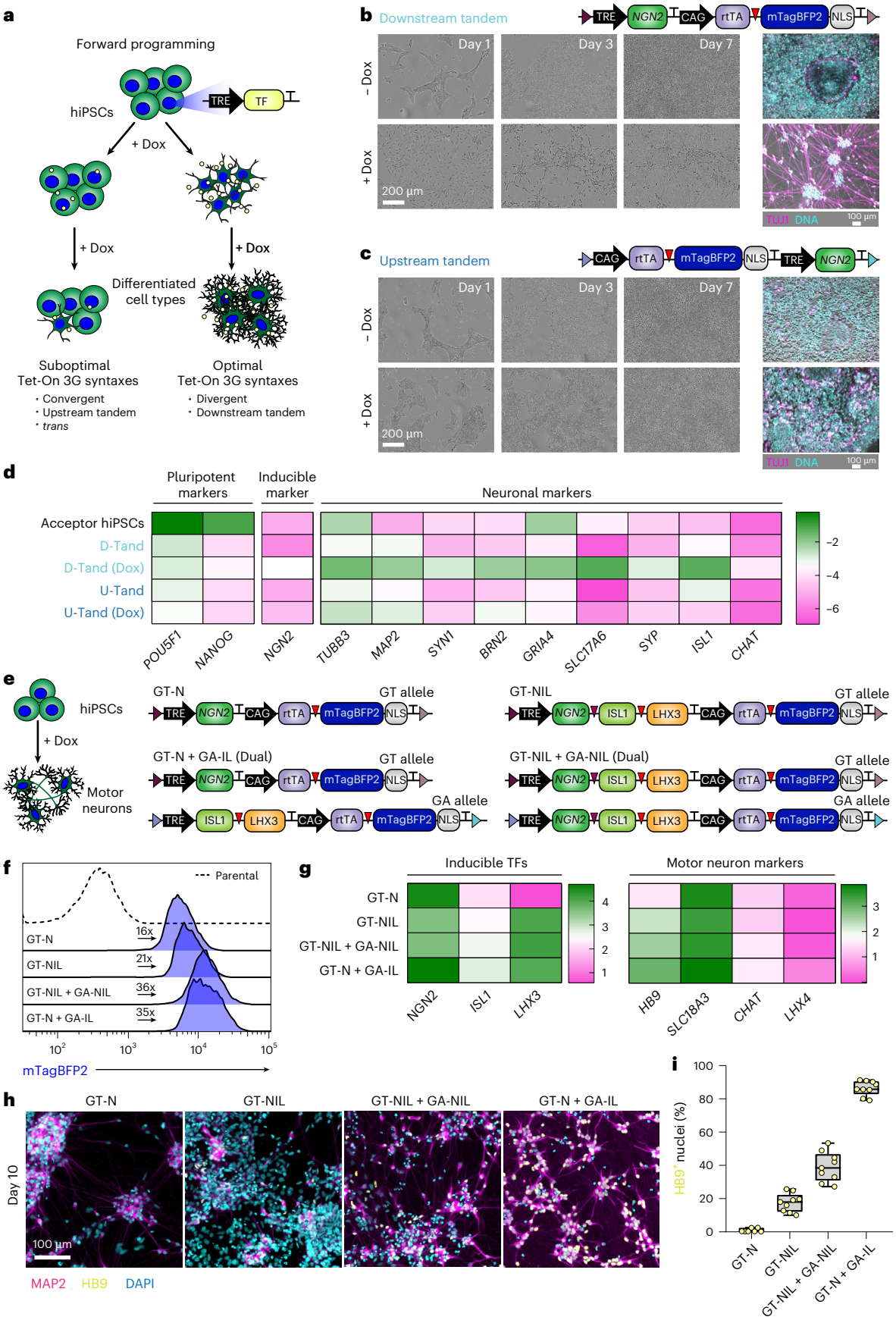

https://doi.org/10.1038/s41551-026-01677-9

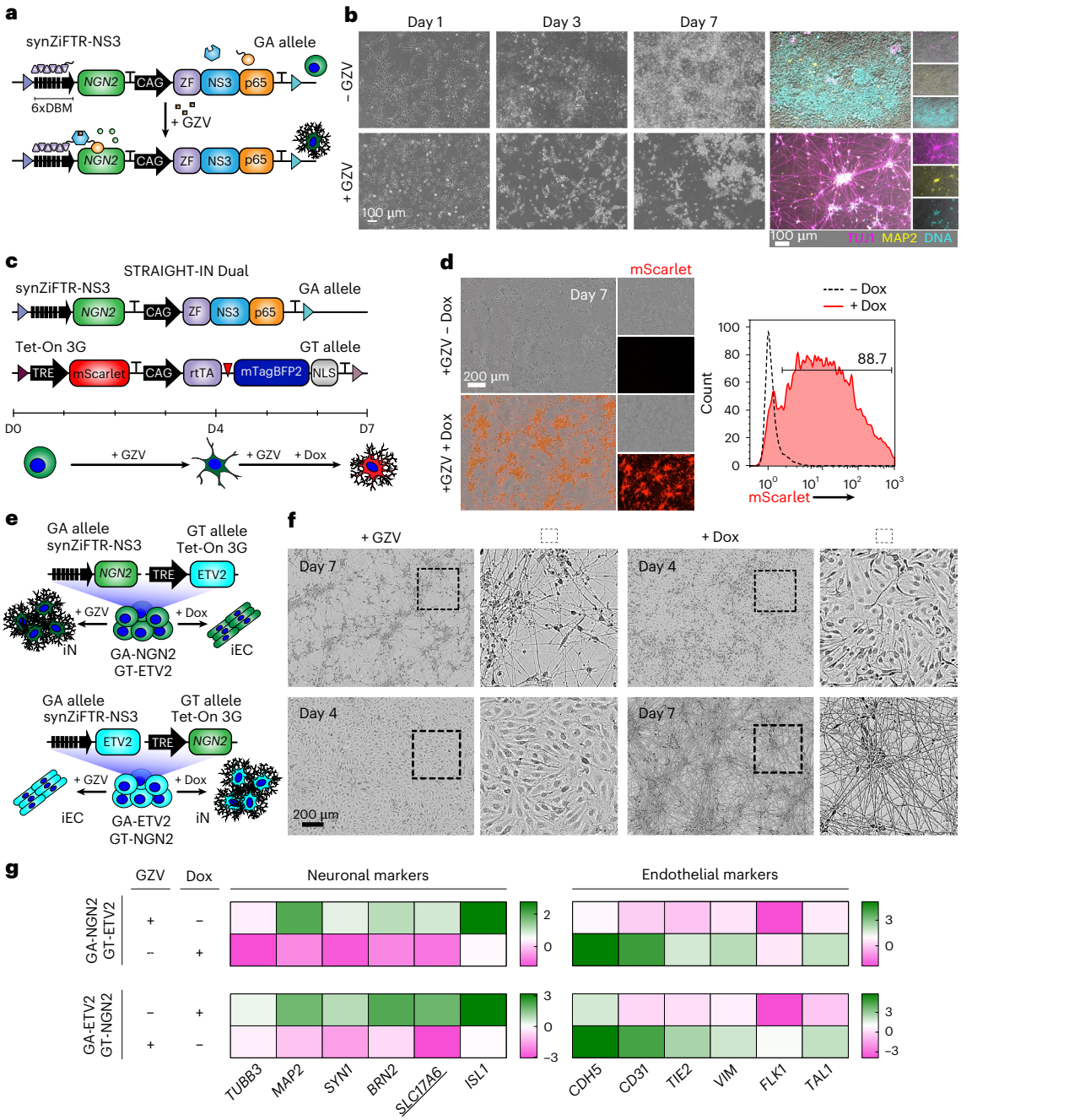

Fig. 6 | Dual-fate programming via orthogonal, inducible transcription factor expression using STRAIGHT-IN Dual. a, Schematic of a downstream tandem synZiFTR-based *NGN2* cassette integrated into the GA allele, enabling grazoprevir-inducible expression. **b**, Phase-contrast and immunofluorescence images of cells at indicated time points, cultured with (+) or without (–) grazoprevir (TUJ1, magenta; MAP2, yellow; DNA, cyan). **c**, Schematic of STRAIGHT-IN Dual hiPSCs with a doxycycline-inducible mScarlet cassette in the GT allele and the grazoprevir-inducible *NGN2* cassette in the GA allele, enabling sequential and combinatorial induction. **d**, Representative fluorescence and phase-contrast images (left), and flow cytometry analysis (right) of grazoprevir-induced iNs cultured with (red line) or without (dashed line) doxycycline. **e**, Schematic of dual-fate STRAIGHT-IN Dual lines with all-in-one downstream tandem inducible *NGN2* or *ETV2* cassettes regulated by synZiFTR (GA allele) or Tet-On 3G (GT allele) systems. **f**, Representative phase-contrast images of hiPSCs directed into iNs or iECs in the presence of either grazoprevir or doxycycline for the indicated days. **g**, Gene expression analysis of neuronal and endothelial markers from the cells in **f**. Values are normalized to *RPL37A* and shown relative to uninduced condition (log_{10}-transformed). $N = 3$ independent differentiations.

To evaluate promoter activity following lineage commitment, we integrated the previously characterized panel of 11 promoters into the GA allele of hiPSC lines harbouring doxycycline-inducible *NGN2* or *ETV2* in the GT allele. This enabled side-by-side comparison of promoter activity in iNs and induced endothelial cells (iECs) (Extended Data Fig. 9).

Promoter behaviour in iNs and iECs largely mirrored that observed in undifferentiated hiPSCs. As in the pluripotent state, the CAG promoter drove strong, uniform mStayGold expression in both iNs and iECs (Extended Data Fig. 9b,c). UbC and β-actin promoters also remained active, producing moderate and low levels of reporter expression, respectively. By contrast, the remaining promoters, including hEF1α, PGK and CBh, either failed to produce detectable reporter signals or showed transgene silencing, consistent with observations in undifferentiated hiPSCs.

Orthogonal inducible systems support dual-fate programming of genetically uniform hiPSCs

To achieve independent control over two cargoes within a single hiPSC line, we introduced a second, orthogonal inducible system alongside Tet-On 3G. We selected a synZiFTR system that couples the ZF10 DNA-binding domain to a grazoprevir-responsive NS3 module and a p65 transcriptional activator[22]. An all-in-one synZiFTR expression cassette was constructed in the downstream tandem configuration and integrated into the GA allele (Extended Data Fig. 10a,b). A 3-day induction of an mGreenLantern reporter in hiPSCs revealed toxicity at grazoprevir concentrations above 250 nM, with 125 nM selected as an optimal concentration that supported transgene induction with minimal cytotoxicity (Extended Data Fig. 10c). At 125 nM grazoprevir, synZiFTR-mediated NGN2 expression efficiently generated TUJ1$^+$MAP2$^+$ iNs within 7 days (Fig. 6a,b).

To demonstrate independent dual gene regulation, we combined both inducible systems using STRAIGHT-IN Dual. *NGN2* was integrated into the GA allele under synZiFTR control, while mScarlet was targeted to the GT allele under Tet-On 3G regulation (Fig. 6c). Grazoprevir was maintained throughout the 7-day differentiation procedure, with doxycycline added from day 3. By day 7, most iNs expressed mScarlet (Fig. 6d and Extended Data Fig. 10d).

To exploit this modularity, we established dual-fate hiPSC lines capable of differentiating into distinct lineages based on inducer choice. In one configuration, *NGN2* expression was controlled by synZiFTR and *ETV2* by Tet-On 3G, while in the other configuration, this arrangement was reversed (Fig. 6e). Exposure to grazoprevir or doxycycline resulted in rapid and efficient differentiation into either iNs or iECs (Fig. 6f). Lineage commitment was confirmed by qPCR and flow cytometry, with grazoprevir-induced iECs expressing CD31 and CD144 (Fig. 6g and Extended Data Fig. 8e). Together, these results highlight the versatility of STRAIGHT-IN Dual for independently controlling multiple transcriptional programmes in a single, genetically uniform hiPSC line, thereby providing a flexible framework for implementing orthogonal gene circuits and for generating mixed or patterned cell populations.

Discussion

In this study, we present STRAIGHT-IN Dual, a platform enabling rapid, efficient and allele-specific integration of two independent DNA payloads into the *CLYBL* locus in hiPSCs. Following protocol optimization, genetically modified hiPSC lines could be generated in less than 1 week, yielding near-uniform edited populations after selection. For the GA allele, integration and excision could be completed within 9 days without cell passaging.

STRAIGHT-IN Dual supports simultaneous integration of two payloads with orthogonal specificity by using the GT and GA Bxb1 recombination sequences[18]. With eeBxb1, a hyperactive Bxb1 variant[9], we achieved higher integration efficiencies than with wild-type Bxb1, most notably at the GA allele. This may reflect the inclusion of *attP*/*attB*-GA sequences in some of the circuits used during the directed evolution of eeBxb1[9], potentially biasing activity towards these sites. However, the precise mechanism by which the central dinucleotide influences recombination efficiency remains unclear and warrants further investigation.

Because Bxb1 catalyses recombination through DNA double-strand break intermediates[35], we also investigated whether transiently suppressing the p53-mediated DNA damage response would improve survival and recovery of edited cells. Co-delivery of p53DD modRNA together with eeBxb1 modRNA increased integration efficiency ~10-fold. These results align with the broader utility of transient p53 interference during genome engineering[16,36,37].

STRAIGHT-IN Dual also supports near-scarless genomic modifications by excising auxiliary elements such as reporters, selection markers and plasmid backbones. Consistent with previous findings[38], removal of auxiliary sequences reduced transgene silencing in both undifferentiated and differentiated hiPSCs, and also could enable reuse of the LPs for subsequent modifications. We achieved near-complete excision from both alleles using plasmid-free strategies (TAT-Cre and Flp-T2A-BleoR modRNA) and streamlined the GA allele workflow to avoid cell passaging. Together, these improvements simplify generation of multiple engineered lines, either individually or pooled, facilitating integration of plasmid libraries and performing combinatorial studies at single-copy resolution. The speed and robustness of the optimized workflow should also support automation-compatible pipelines for larger-scale functional screens.

Dual integration of the same payload into both alleles approximately doubled transgene expression, indicating that both LPs perform comparably. We recently showed that uniform biallelic integration is critical for high-resolution genome folding profiling and enables precise measurements of transcriptional activation effects on chromatin architecture[39].

Our work also highlights limitations of commonly used molecular tools used in hiPSCs. The widely used hEF1α promoter underwent rapid silencing, consistent with earlier studies[40]. To identify sequences that better resist silencing, we screened a library of 11 promoters using both individual and pooled integrations. The pooled format recapitulated the behaviours observed in individually engineered lines, indicating that STRAIGHT-IN Dual can support scalable characterization of regulatory elements.

Although transient assays initially showed detectable transgene expression from all promoters, more than half exhibited substantial silencing after single-copy integration. Viral promoters (CMV, RSV and SV40), shortCAG and CpG-free were rapidly silenced, while PGK and hEF1α showed progressive silencing. By contrast, CAG, CBh, UbC and β-actin promoters maintained stable reporter expression at the *CLYBL* locus in hiPSCs with extended passaging, although only CAG maintained long-term activity at the *AAVS1* locus. Across forward-programmed iNs and iECs, promoter behaviours largely mirrored those observed in undifferentiated hiPSCs, with CAG, UbC and β-actin remaining active in cell types derived from distinct germ layers.

The stability of the full-length CAG promoter likely arises from its composite architecture, combining the cytomegalovirus (CMV) immediate-early enhancer with the chicken β-actin promoter (including its first intron) and a rabbit β-globin splice acceptor[41]. These elements provide multiple transcription factor binding sites and can recruit chromatin remodellers to help resist DNA methylation[42]. By contrast, truncated variants (CBh and shortCAG) and CMV alone lack one or more of these features and showed reduced resistance to silencing. Nonetheless, the large size and high GC content of CAG complicates cloning, highlighting the need to develop and evaluate alternative synthetic promoters that retain the stable expression characteristics of CAG while improving ease of use. STRAIGHT-IN Dual provides a locus-controlled platform to screen promoter sequence libraries and to evaluate additional regulatory elements to mitigate transgene silencing in hiPSCs and their derivatives[43–45].

We also used STRAIGHT-IN Dual to systematically analyse gene syntax in the all-in-one Tet-On 3G system, identifying the divergent and downstream tandem syntaxes as the most effective configurations for induction. These syntaxes are commonly favoured in mammalian systems[46–50], whereas convergent and upstream tandem syntaxes typically perform poorly unless extensively optimized[51,52]. Consistent with this, NGN2 expressed from the downstream tandem syntax supported efficient forward programming of hiPSCs into iNs, whereas the upstream tandem configuration produced few iNs. This is consistent with an upstream dominance effect driven by supercoiling-mediated feedback, which can regulate the expression of neighbouring genes in a syntax-specific manner[39]. The downstream tandem design also supported ETV2-driven differentiation of hiPSCs to iECs within 4 days. While similar outcomes have been reported using hyperactive

transposase systems, those strategies typically involve random integration of many copies of the construct, increasing the risk of unintended genomic disruption[53,54]. Our results indicate that a single, site-specific integration of *ETV2* can be sufficient to forward programme most of the population into iECs, and suggests that high transgene copy numbers are not required when expression is appropriately configured and controlled.

Our comparative analysis of motor neuron forward programming strategies further demonstrates that transcript architecture and allelic arrangement strongly influence transcription factor expression and downstream differentiation. Reconfiguring the single-allele expression cassette either as three separate inducible transcription units in downstream tandem orientation, or as two units in a divergent syntax, did not improve transcription factor output or iMN conversion relative to the single tricistronic NIL cassette[55]. As expected, introducing a second NIL cassette into the other allele increased overall expression in a predictable, copy number-dependent manner, but still did not achieve differentiation efficiencies comparable to the split-allele GT-N + GA-IL design. The GT-N + GA-IL line consistently showed superior induction of motor neuron markers and the highest proportion of HB9$^+$ cells, possibly because it avoids position effects common to 2A-linked polycistronic constructs[56]. Future work should identify improved design strategies for multicistronic cassettes that overcome these limitations. More broadly, STRAIGHT-IN Dual enables systematic screening of transcription factor combinations and configurations for lineage specification, providing an alternative to pooled viral strategies that offer limited control over transcription factor stoichiometry[48,57].

Finally, we demonstrate that STRAIGHT-IN Dual supports combinatorial and sequential control of transgenes using independent inducible systems, exemplified here by Tet-On 3G and the GZV-responsive synZiFTR system. This enabled precise temporal control of both reporters and lineage-specifying transcription factors. Using this framework, we generated dual-fate programmable hiPSC lines that could be directed towards neuronal or endothelial lineages based on inducer choice. Previous multi-fate approaches have typically relied on mixing or patterning genetically distinct cell populations[58]. By contrast, our strategy enables specification of distinct fates from a single engineered line using small-molecule control, creating opportunities for spatial patterning without the need for complex bioprinting. The platform should also enable coupling cell-fate programming with independent expression of biosensors or inducible modelling of sporadic/acquired mutations in differentiated cells. Furthermore, these inducible DNA payloads can be expressed in more complex in vitro systems, such as organoids, organs-on-chips and 3D tissue constructs, expanding opportunities for cell-based modelling and engineered tissue design.

Some limitations of the current study should be acknowledged. First, all engineered hiPSC lines were derived from a single parental clone, which reduces variability but limits the immediate generalizability of our findings. Validation across additional donor backgrounds is therefore warranted, and STRAIGHT-IN Dual LPs are currently being targeted into additional hiPSC lines. Second, most payloads were integrated at *CLYBL*, with limited comparisons at *AAVS1*, so locus-specific effects cannot be excluded. Third, the transgene sequence can influence transgene silencing[59]. Here promoter activity was primarily assessed using fluorescent reporters. Broader testing with additional relevant payload classes will be important to refine design rules for stable expression.

In summary, STRAIGHT-IN Dual enables rapid generation of precisely engineered hiPSC lines with dual, orthogonal genetic control. The platform supports scalable screening, combinatorial interrogation of transcriptional unit designs and inducible control of cell fate, and should be a useful toolkit for biomedical and synthetic biology research in human stem cells.

Methods

hiPSC culture

hiPSCs were maintained in StemFlex Medium (ThermoFisher) or mTeSR Plus Medium (STEMCELL Technologies) on tissue culture plates coated with Laminin-521 (BioLamina or STEMCELL Technologies) at 1.5 μg cm^{-2}. Cells were passaged twice weekly using either 1× TrypLE Select (ThermoFisher) or Gentle Cell Dissociation Reagent (STEMCELL Technologies). For trilineage differentiation, hiPSCs were seeded on 96-well imaging plates (Corning) and differentiated using the STEMdiff Trilineage Differentiation Kit (STEMCELL Technologies) according to the manufacturer's instructions.

Construction of bxb1-GA *attP* LP targeting plasmid

To generate the CLYBL-Bxb1-LP-Dual-TC plasmid (Addgene #229776), the CLYBL-Bxb1-LP-v2-TC plasmid (Addgene #194327) was first digested with NheI and PmeI (both NEB). An LP fragment (composed of an *FRT* site, PGK promoter, mScarlet reporter, GA *attP* site, a puromycin resistance gene lacking an initiation codon (**PuroR*) and an *F3* site) was PCR-amplified from a separate plasmid source. The *CLYBL* right homology arm (R-HA) fragment was PCR-amplified from CLYBL-Bxb1-LP-v2-TC. All fragments were amplified using PrimeSTAR Max DNA Polymerase (Takara Bio), treated with DpnI (NEB), purified using the Wizard SV Gel and PCR Clean-Up System kit (Promega), and assembled using the NEBuilder HiFi DNA Assembly Cloning Kit (NEB).

Generation of STRAIGHT-IN Dual hiPSC line

To generate the STRAIGHT-IN Dual hiPSC line (Supplementary Fig. 5), the GA-specific LP plasmid (CLYBL_Bxb1-GA_LP_Dual_TC) was targeted to the second *CLYBL* allele in LU99_CLYBL-bxb-v2 hiPSCs (hPSCreg, LUMCi004-A-2; RRID:CVCL_C6UD). Cells were co-transfected with 500 ng targeting plasmid and 500 ng each of the TALEN expression vectors pZT-C13-L1 and pZT-C13-R1 (Addgene #62196 and #62197)[19] using Lipofectamine Stem Transfection Reagent (ThermoFisher), according to the manufacturer's instructions.

Following recovery and expansion, mScarlet$^+$ cells were clonally isolated using the single-cell deposition function of a BD FACSAria III (BD Biosciences). Clones were expanded and putative targeted clones (52/54; 94.5% targeting efficiency) were identified by PCR screening of the 5′ junction, followed by PCR screening of the 3′ junction and by Sanger sequencing. Primer sequences (IDT) are listed in Supplementary Table 1.

The resulting LU99_CLYBL-bxb-v3_Dual hiPSC line (STRAIGHT-IN Dual; hPSCreg, LUMCi004-A-8) was assessed for pluripotency marker expression, trilineage differentiation potential, mycoplasma contamination and genomic integrity by G-banding and the iCS-digital PSC 24-probes kit (Stemgenomics). Alkaline phosphatase staining was performed using the Alkaline Phosphatase Detection Kit (Merck) according to the manufacturer's instructions.

Donor plasmid assembly

Donor plasmids containing genes of interest were assembled using NEBuilder HiFi (NEB) or Golden Gate cloning[60], as previously described[38,61,62]. For Tet-On 3G payloads, the Bxb1-GT_AIO-TetOn_Down-Tandem Donor plasmid (Addgene #229783) was digested with NotI (NEB), genes of interest were amplified from source templates by PCR, and inserts were assembled into the linearized donor using HiFi. Blue-white screening was performed by supplementing LB agar plates with X-Gal (20 μg ml^{-1}; ThermoFisher). A similar strategy was used for the synZiFTR donor plasmid (Bxb1-GA_AIO-GZV-SynZiFTR_Down-Tandem donor; Addgene #229787). This plasmid was assembled from fragments PCR-amplified from pMN-334 (Addgene #195468). For the promoter panel, promoter sequences were PCR-amplified from the following plasmids: CMV (Addgene #40651), SV40 (Addgene #229779), RSV (Addgene #12253), PGK (Addgene #229776), CpG-free (Addgene

#96945), shortCAG (Addgene #238347), hEF1α (Addgene #229779), CAG (Addgene #229790), UbC (Addgene #20342), CBh (Addgene #62988) and β-actin (Addgene #13680). Promoter fragments were cloned upstream of mStayGold in a linearized vector using HiFi or Golden Gate cloning.

In vitro transcription

Plasmid templates used for modRNA synthesis contained the 5′-UTR of human β-globin, a Kozak sequence, the coding sequence of the protein of interest and the 3′-UTR of human β-globin. Linear templates for in vitro transcription were generated by PCR using Q5 DNA Polymerase (NEB) with a forward primer encoding a T7 promoter compatible with CleanCap AG reagent (uppercase bases; TriLink BioTechnologies) and annealing to the 5′-UTR (lower-case bases), and a reverse primer encoding a poly(A) tract and annealing to the 3′-UTR. Primer sequences were as follows: forward, 5′-AGCTATAATACGACTCACTATAAGctcctgggcaacgtgctg-3′; reverse, 5′-poly(T)$_{116}$-GCAATGAAAATAAATGTTTTTTATTAGGCAGAAT-3′.

PCR products were gel-purified (1% agarose gel) and extracted using the Monarch PCR and DNA Cleanup Kit (NEB). For in vitro transcription, 200 ng of the PCR product was transcribed in a 20 µl reaction using the HiScribe T7 High Yield RNA Synthesis Kit (NEB), substituting UTP with N1-methylpseudouridine-5′-phosphate (TriLink BioTechnologies) and co-transcriptionally capping with CleanCap Reagent AG. Reactions were incubated at 37 °C for 2–4 h, diluted to 50 µl, treated with 2 µl DNase I (ThermoFisher) at 37 °C for 30 min and purified using the 50 µg Monarch RNA Cleanup Kit (NEB). modRNAs were eluted in 60 µl nuclease-free water, quantified by spectrophotometry and stored at −80 °C.

Donor plasmid integration and enrichment

Unless otherwise stated, donor plasmids (300 ng cm^{-2}) were co-transfected into CLYBL-bxb-v3 Dual hiPSCs with either 400 ng of a Bxb1 expression plasmid (pCAG-NLS-HA-Bxb1; Addgene #51271)[63] or (ee)Bxb1 modRNA, using Lipofectamine Stem Transfection Reagent. For the standard workflow, 3–4 days after transfection, hiPSCs were collected and reseeded (~5 × 10^5 cells per well) in 12-well plates. The next day, zeocin (15 µg ml^{-1}; ThermoFisher) or puromycin (1 µg ml^{-1}; InvivoGen) was added to the culture medium for 3 days. For the STRAIGHT-IN rapid protocol, zeocin or puromycin selection was added to the culture medium 1 day post-transfection and maintained for 3 days. Donor plasmid integration was confirmed by ddPCR using *attP*/*attR* assays for the GT allele and GA alleles, as previously described[38].

Auxiliary element excision

hiPSCs containing integrated payloads were seeded at 2 × 10^5 cells per well in 24-well plates. The following day, cells were transfected using Lipofectamine Stem Transfection Reagent with 400 ng of StemMACS Cre Recombinase or StemMACS Flp Recombinase modRNA (Miltenyi Biotec).

For Flp-mediated excision coupled to selection, Flp-T2A-BleoR modRNA (500 ng per well) was transfected and zeocin selection (15 µg ml^{-1}) initiated 24 h later and maintained for 3 days. Alternatively, TAT-Cre protein (1 µM) was added to the culture medium 1 day after passaging and maintained for 24 h, as previously described[38].

At ~80% confluence (~2–3 days after transfection), the hiPSCs were passaged for continued culture, with the remainder used for genomic DNA (gDNA) extraction.

gDNA extraction

gDNA from hiPSCs cultured in 96-well plates was extracted using QuickExtract (Lucigen). gDNA from hiPSCs cultured in 24- or 12-well plates was extracted using the High Pure PCR Template Preparation Kit (Roche) or the DNeasy Blood & Tissue Kit (QIAGEN), according to the manufacturer's instructions.

ddPCR

ddPCR was performed and analysed using a thermocycler, the Q200 AutoDG and QX200 Droplet Digital PCR System, and QuantaSoft software (all Bio-Rad), as previously described[38]. For all reactions, ~100 ng gDNA was digested with HindIII (NEB). For copy number assays, the autosomal gene *RPP30* was used as a reference. Primer and probe sequences are listed in Supplementary Table 2.

DNA library preparation, bead cleanup and NGS analysis

Promoter sequences were PCR-amplified from 100 ng gDNA using the NEBNext High-Fidelity 2× PCR Master Mix (NEB). Primer sequences and annealing temperatures are listed in Supplementary Table 3. Cycling conditions were 98 °C for 30 s, 14 cycles of 98 °C for 10 s, annealing at the specified temperature for 30 s and extension at 72 °C for 30 s, followed by 72 °C for 2 min.

PCR products were purified using AMPure XP beads (Beckman Coulter) at a 1:1 bead-to-sample volume ratio. Samples were incubated for 10 min at room temperature and placed on a magnetic stand for 5 min, after which the supernatant was removed. Beads were washed twice with 80% ethanol (30 s each). After brief centrifugation, residual ethanol was removed and beads were air-dried on the magnetic stand for 10 min. Beads were incubated in nuclease-free water for 5 min, and DNA eluted on the magnetic stand (5 min).

A second PCR was performed to add Illumina TruSeq small RNA adapters under the same thermocycling conditions, with annealing at 60 °C. Final libraries were cleaned using two bead purifications at 1:1 and 0.9:1 bead-to-sample volume ratios. Libraries were sequenced on an Illumina MiSeq platform using 300 bp paired-end reads. Reads were aligned to a custom reference containing all expected promoter amplicons using BWA-MEM (v0.7.17) with default parameters. Read counts for each promoter were determined independently from Read 1 and Read 2, yielding highly concordant results.

Cardioid differentiation

Cardioids were generated as previously described[64] with minor adaptations. hiPSCs were collected and 5 × 10^4 cells per well were seeded in U-bottom 96-well ultra-low attachment plates (PrimeSurface) in 200 µl of mBEL medium[65] containing 4 µM CHIR99021 (Axon Medchem), 30 ng ml^{-1} FGF-2 (Miltenyi Biotec), 5 µM LY294002 (Tocris), 50 ng ml^{-1} Activin A (Miltenyi Biotec), 10 ng ml^{-1} BMP4 (R&D Systems), 1 µg ml^{-1} human insulin (Gibco) and 1× CEPT cocktail[66]. After 40 h, medium was replaced with 200 µl of mBEL medium containing 8 ng ml^{-1} FGF-2, 10 ng ml^{-1} BMP4, 10 µg ml^{-1} human insulin, 0.25 µM IWPL6 (Abmole), 5 µM XAV939 (Tocris) and 0.05 µM retinoic acid (Sigma-Aldrich). Cardioids were refreshed daily until day 7, and then maintained in mBEL containing 10 µg ml^{-1} human insulin with medium refreshment every other day. Doxycycline (1 µM; ThermoFisher) was added as specified in Fig. 4f. On day 14, cardioids from the same condition were pooled, dissociated to single cells using 5× TrypLE for 10 min at 37 °C and filtered. Data were acquired using a MacsQuant VYB (Miltenyi Biotec).

Forward programming

hiPSC lines were dissociated as described above and plated in Laminin-521-coated 24-well plates at 2.5 × 10^4 cells per well.

Forward programming to iNs was initiated on the day of passage as described elsewhere[6]. In brief, induction was performed in DMEM/F12 containing L-glutamine (Corning), non-essential amino acids (1×; Gibco), N2 supplement (1×; Fisher Scientific), penicillin/streptomycin (1×; Fisher Scientific) and doxycycline (1 µM). After 2 days, medium was replaced with Neurobasal Medium (Gibco) supplemented with Glutamax supplement (1×; Gibco), non-essential amino acids, B27 supplement (1×; Gibco), N2 supplement, BDNF (10 ng ml^{-1}; Peprotech), NT3 (10 ng ml^{-1}; Peprotech), penicillin/streptomycin and doxycycline (1 µM). For synZiFTR-based induction, grazoprevir (125 nM;

MedChemExpress) was added for 7 days. Where indicated, EdU (40 µM) was added from day 3 for 48 h.

Forward programming to iMNs was performed similarly, except that doxycycline (1 µM) was maintained for 10 days. For the GT-NIL line, EdU (40 µM) was additionally applied from day 3 to day 5.

Forward programming to iECs was initiated on the day of passage in human endothelial SFM medium (Invitrogen) containing human platelet-poor plasma (1×; Sigma-Aldrich), FGF (20 ng ml^{-1}; Miltenyi Biotec), VEGF (30 ng ml^{-1}; Miltenyi Biotec) and penicillin/streptomycin (1×), with doxycycline (1 µM) added for 3 days. For synZiFTR-based induction, grazoprevir (500 nM) was used instead of doxycycline.

RNA extraction, cDNA synthesis and RT–qPCR

RNA was extracted using the NucleoSpin RNA kit (Macherey-Nagel) and reverse-transcribed using the iScript cDNA synthesis kit (Bio-Rad). qPCR mixtures were prepared using iQ SYBR Green Supermix (Bio-Rad) and run on a CFX Opus 384 Real-Time PCR System (Bio-Rad). Data were analysed using the ΔC_t method. C_t values were normalized to *RPL37A* and $\log_{10}$-transformed. Primer sequences are listed in Supplementary Table 4.

Flow cytometry analysis

Single-cell suspensions were obtained using 1× TrypLE Select and filtered to remove aggregates. hiPSCs were fixed and permeabilized using the FIX and PERM Cell Permeabilization Kit (ThermoFisher), according to the manufacturer's instructions. Data were acquired using a MacsQuant VYB (Miltenyi Biotec) or Attune NxT (ThermoFisher) flow cytometer and analysed using FlowJo (v10.2). An example of the gating strategy is shown in Supplementary Fig. 6.

Immunocytochemistry staining

Cells were fixed in 4% paraformaldehyde (ThermoFisher) in phosphate-buffered saline without Ca^{2+} and Mg^{2+} ($PBS^{-/-}$) for 10 min at room temperature. Cells were then permeabilized and blocked using either $PBS^{+/+}$ containing 0.05% Triton X-100 (Merck) and 10% fetal calf serum, or $PBS^{-/-}$ containing 5% fetal bovine serum and 0.5% Tween-20. Primary antibody incubations were performed overnight at 4 °C followed by $PBS^{-/-}$ washes and incubation with the appropriate conjugated secondary antibodies where required. For 96-well formats, primary and secondary antibody incubations were performed in 70 µl per well, with washes performed in 100 µl $PBS^{-/-}$. Nuclei were counterstained with DAPI (0.1 µg ml^{-1}; ThermoFisher).

Images were acquired using an EVOS M7000 (ThermoFisher) at 20× magnification, a Keyence BZ-X800 fluorescence microscope or a Dragonfly high-speed confocal microscope (Andor) at 40× magnification.

Antibodies

The following antibodies were used: BV421 mouse anti-OCT3/4 (dilution 1:25, BD Biosciences #565644), PE mouse anti-human NANOG (1:50, BD Biosciences #560483), PE-Vio770 anti-human SSEA4 (1:25, Miltenyi Biotec #30-121-348), FITC anti-human CD31 (1:50, Miltenyi Biotec #130-117-390), APC rat anti-mouse CD31 (1:100, Invitrogen #50-149-40), Alexa Fluor 488 mouse anti-human CD144 (1:50, Invitrogen #53-1449-42), PE anti-human CD144 (1:50, Miltenyi Biotec #130-135-356), Alexa Fluor 555 rabbit anti-human FOXA2 (1:500, Cell Signaling Technology (CST) #50079), Alexa Fluor 647 rabbit anti-human GATA4 (1:200, CST #66309), Alexa Fluor 488 mouse anti-human Nestin (1:200, CST #35884), Alexa Fluor 647 rabbit anti-human PAX6 (1:200, CST #60433), Alexa Fluor 488 rabbit anti-human brachyury (1:200, CST #94663), Alexa Fluor 647 rabbit anti-human vimentin (1:400, CST #9856), rabbit anti-human MAP2 (1:500, CST #4542), mouse anti-rat TUBB3 (1:500, BioLegend #801201), mouse anti-chicken MNX1/HB9 (1:10, DSHB #81.5C10), sheep anti-human CD31 (1:200, R&D Systems #AF806), mouse anti-human ZO-1 (1:200, Invitrogen #33-9100), Alexa Fluor 488 donkey anti-mouse IgG (1:500, ThermoFisher #A-21202), Alexa Fluor 594 donkey anti-rabbit IgG (1:500, ThermoFisher #A-21207), Alexa Fluor 647 donkey anti-mouse IgG (1:500, ThermoFisher #A-31571), Alexa Fluor 647 donkey anti-sheep IgG (1:500, ThermoFisher #A-21448) and Alexa Fluor 647 donkey anti-rabbit IgG (1:300, ThermoFisher #A-31573).

Live-cell imaging and calcium recordings

Live imaging of fluorescent reporter gene expression was performed using a BZ-X810 (10× or 20× magnification), an Incucyte S3 live-cell analysis system (10×, Sartorius) or a Dragonfly high-speed confocal (40×) microscope. For intracellular calcium recordings, 20 s time-lapse videos were acquired on day 9 using a BZ-X810 microscope at 10× magnification with a frame rate of 10 frames per second. Calcium transients were analysed in ImageJ (NIH, v1.54p), and intensity traces were extracted from three user-defined regions of interest.

Viability imaging of iMNs

Live-cell imaging of iMNs was performed using calcein AM (Invitrogen). Cells were incubated with calcein AM (5 µM) for 30 min at 37 °C, washed with $PBS^{-/-}$ and imaged at 10× magnification using an EVOS Auto2 microscope (ThermoFisher). For nuclear and viability staining, iMNs were also incubated with Hoechst 33342 (5 µg ml^{-1}; Invitrogen) and propidium iodide (10 µg ml^{-1}; Merck) for 1 h at 37 °C, washed with $PBS^{-/-}$ and imaged using the same settings.

Quantification of iMNs

The TWOMBLI plug-in[67] for ImageJ (v1.54p) was adapted to quantify total dendritic area, the number of branching points and overall dendritic length of iMNs stained with calcein AM. TWOMBLI identified dendritic extensions by mapping ridgelines after thresholding of calcein AM-stained images using predefined parameters. Total dendritic length was calculated as the sum of all masked fibre lengths per image, and branch points were defined as the number of fibre intersections per image.

In parallel, a custom CellProfiler pipeline was developed to quantify Hoechst- and propidium iodide-stained nuclei. Propidium iodide-postive nuclei were masked over $Hoechst^+$ nuclei to remove co-localized signals, enabling quantification of surviving ($Hoechst^+$) nuclei. Survival was calculated as the percentage of $Hoechst^+$ nuclei relative to total nuclei.

For quantification of HB9 and DAPI signals, a second custom CellProfiler pipeline was used. RGB images were split into individual channels, followed by intensity rescaling and a light Gaussian blur to reduce noise. Nuclei were segmented from the processed images using intensity-based thresholding, enabling the separation of clustered objects. $HB9^+$ nuclei were identified and masked over the DAPI channel to identify the $HB9^-$ population. The total number of $HB9^+$ nuclei was used to calculate the percentage of HB9-expressing cells per image.

Statistics and reproducibility

Statistical analyses were performed using GraphPad Prism (v10.6.1). Sample sizes and statistical analyses are shown in the figure legends. Genetically modified hiPSC populations for each fluorescent reporter or transcription factor construct were generated and used as bulk (non-clonally isolated) cultures. The number of independent differentiation experiments and technical replicates are shown in the figure legends.

Ethics statement

The medical ethics committee (Leiden University Medical Center) approved the use of the hiPSC lines in this study (approval number P13.080).

Reporting summary

Further information on research design is available in the Nature Portfolio Reporting Summary linked to this article.

Data availability

All raw data that support this study are available via Zenodo at https://zenodo.org/records/17930642 (ref. 68). DNA sequencing data generated in this study have been deposited in the European Nucleotide Archive (ENA) under accession code PRJEB108223. Plasmids generated in this study have been deposited on Addgene (https://www.addgene.org/browse/article/28252243/). hiPSC lines are available under an MTA. Requests should be directed to R.P.D. Source data are provided with this paper.

Code availability

The code used for image analysis (CellProfiler pipelines) and for processing promoter sequencing reads is available via Zenodo at https://zenodo.org/records/17930642 (ref. 68).

References

1. Balmas, E. et al. Manipulating and studying gene function in human pluripotent stem cell models. *FEBS Lett.* **597**, 2250–2287 (2023).
2. Blanch-Asensio, A. et al. STRAIGHT-IN enables high-throughput targeting of large DNA payloads in human pluripotent stem cells. *Cell Rep. Methods* **2**, 100300 (2022).
3. Brandão, K. O. et al. Isogenic sets of hiPSC-CMs harboring distinct KCNH2 mutations differ functionally and in susceptibility to drug-induced arrhythmias. *Stem Cell Rep.* **15**, 1127–1139 (2020).
4. Hosur, V., Low, B. E. & Wiles, M. V. Programmable RNA-guided large DNA transgenesis by CRISPR/Cas9 and site-specific integrase Bxb1. *Front. Bioeng. Biotechnol.* **10**, 910151 (2022).
5. Low, B. E., Hosur, V., Lesbirel, S. & Wiles, M. V. Efficient targeted transgenesis of large donor DNA into multiple mouse genetic backgrounds using bacteriophage Bxb1 integrase. *Sci. Rep.* **12**, 5424 (2022).
6. Pawlowski, M. et al. Inducible and deterministic forward programming of human pluripotent stem cells into neurons, skeletal myocytes, and oligodendrocytes. *Stem Cell Rep.* **8**, 803–812 (2017).
7. Zhang, M., Yang, C., Tasan, I. & Zhao, H. Expanding the potential of mammalian genome engineering via targeted DNA integration. *ACS Synth. Biol.* **10**, 429–446 (2021).
8. Anzalone, A. V. et al. Programmable deletion, replacement, integration and inversion of large DNA sequences with twin prime editing. *Nat. Biotechnol.* **40**, 731–740 (2022).
9. Pandey, S. et al. Efficient site-specific integration of large genes in mammalian cells via continuously evolved recombinases and prime editing. *Nat. Biomed. Eng.* **9**, 22–39 (2025).
10. Yarnall, M. T. N. et al. Drag-and-drop genome insertion of large sequences without double-strand DNA cleavage using CRISPR-directed integrases. *Nat. Biotechnol.* **41**, 500–512 (2023).
11. Brosh, R. et al. A versatile platform for locus-scale genome rewriting and verification. *Proc. Natl Acad. Sci. USA* **118**, e2023952118 (2021).
12. Mitchell, L. A. et al. De novo assembly and delivery to mouse cells of a 101 kb functional human gene. *Genetics* **218**, iyab038 (2021).
13. Pinglay, S. et al. Synthetic regulatory reconstitution reveals principles of mammalian *Hox* cluster regulation. *Science* **377**, eabk2820 (2022).
14. Duportet, X. et al. A platform for rapid prototyping of synthetic gene networks in mammalian cells. *Nucleic Acids Res.* **42**, 13440–13451 (2014).
15. Roelle, S. M., Kamath, N. D. & Matreyek, K. A. Mammalian genomic manipulation with orthogonal Bxb1 DNA recombinase sites for the functional characterization of protein variants. *ACS Synth. Biol.* **12**, 3352–3365 (2023).
16. Rosenstein, A. et al. FAST-STEM: a human pluripotent stem cell engineering toolkit for rapid design-build-test-learn development of human cell-based therapeutic devices. Preprint at *bioRxiv* https://doi.org/10.1101/2024.05.23.595541 (2024).
17. Matreyek, K. A., Stephany, J. J. & Fowler, D. M. A platform for functional assessment of large variant libraries in mammalian cells. *Nucleic Acids Res.* **45**, e102–e102 (2017).
18. Jusiak, B. et al. Comparison of integrases identifies Bxb1-GA mutant as the most efficient site-specific integrase system in mammalian cells. *ACS Synth. Biol.* **8**, 16–24 (2019).
19. Cerbini, T. et al. Transcription activator-like effector nuclease (TALEN)-mediated CLYBL targeting enables enhanced transgene expression and one-step generation of dual reporter human induced pluripotent stem cell (iPSC) and neural stem cell (NSC) lines. *PLoS ONE* **10**, e0116032 (2015).
20. Li, J., Li, Y., Pawlik, K. M., Napierala, J. S. & Napierala, M. A CRISPR-Cas9, Cre- *lox*, and Flp- *FRT* cascade strategy for the precise and efficient integration of exogenous DNA into cellular genomes. *CRISPR J.* **3**, 470–486 (2020).
21. Rai, K. et al. Ultra-high-throughput mapping of genetic design space. *Nature* https://doi.org/10.1038/s41586-025-09933-9 (2026).
22. Li, H.-S. et al. Multidimensional control of therapeutic human cell function with synthetic gene circuits. *Science* **378**, 1227–1234 (2022).
23. Blanch-Asensio, A. et al. Generation of AAVS1 and CLYBL STRAIGHT-IN v2 acceptor human iPSC lines for integrating DNA payloads. *Stem Cell Res.* **66**, 102991 (2023).
24. Haideri, T. et al. Robust genome editing via modRNA-based Cas9 or base editor in human pluripotent stem cells. *Cell Rep. Methods* **2**, 100290 (2022).
25. Hew, B. E. et al. Directed evolution of hyperactive integrases for site specific insertion of transgenes. *Nucleic Acids Res.* **52**, e64 (2024).
26. Peterman, E. L., Ploessl, D. S. & Galloway, K. E. Accelerating diverse cell-based therapies through scalable design. *Annu. Rev. Chem. Biomol. Eng.* **15**, 267–292 (2024).
27. Cabrera, A. et al. The sound of silence: transgene silencing in mammalian cell engineering. *Cell Syst.* **13**, 950–973 (2022).
28. Seczynska, M., Bloor, S., Cuesta, S. M. & Lehner, P. J. Genome surveillance by HUSH-mediated silencing of intronless mobile elements. *Nature* **601**, 440–445 (2022).
29. Dou, Y. et al. The CAG promoter maintains high-level transgene expression in HEK293 cells. *FEBS Open Bio* **11**, 95–104 (2021).
30. Zhang, H. et al. Bright and stable monomeric green fluorescent protein derived from StayGold. *Nat. Methods* **21**, 657–665 (2024).
31. Engreitz, J. M. et al. Local regulation of gene expression by lncRNA promoters, transcription and splicing. *Nature* **539**, 452–455 (2016).
32. Johnstone, C. P. & Galloway, K. E. Supercoiling-mediated feedback rapidly couples and tunes transcription. *Cell Rep.* **41**, 111492 (2022).
33. Patel, H. P. et al. DNA supercoiling restricts the transcriptional bursting of neighboring eukaryotic genes. *Mol. Cell* **83**, 1573–1587. e8 (2023).
34. Zhang, Y. et al. Rapid single-step induction of functional neurons from human pluripotent stem cells. *Neuron* **78**, 785–798 (2013).
35. Xu, Z. et al. Accuracy and efficiency define Bxb1 integrase as the best of fifteen candidate serine recombinases for the integration of DNA into the human genome. *BMC Biotechnol.* **13**, 87 (2013).
36. Haideri, T., Lin, J., Bao, X. & Lian, X. L. MAGIK: a rapid and efficient method to create lineage-specific reporters in human pluripotent stem cells. *Stem Cell Rep.* **19**, 744–757 (2024).
37. Li, M. et al. Transient inhibition of p53 enhances prime editing and cytosine base-editing efficiencies in human pluripotent stem cells. *Nat. Commun.* **13**, 6354 (2022).

38. Blanch-Asensio, A., Grandela, C., Mummery, C. L. & Davis, R. P. STRAIGHT-IN: a platform for rapidly generating panels of genetically modified human pluripotent stem cell lines. *Nat. Protoc.* **21**, 429–472 (2026).
39. Johnstone, C. P. et al. Gene syntax defines supercoiling-mediated transcriptional feedback. *Science* **392**, eadw1925 (2026).
40. Bertero, A. et al. Optimized inducible shRNA and CRISPR/Cas9 platforms for in vitro studies of human development using hPSCs. *Development* **143**, 4405–4418 (2016).
41. Hitoshi, N., Ken-ichi, Y. & Jun-ichi, M. Efficient selection for high-expression transfectants with a novel eukaryotic vector. *Gene* **108**, 193–199 (1991).
42. Brown, A. J., Sweeney, B., Mainwaring, D. O. & James, D. C. Synthetic promoters for CHO cell engineering. *Biotechnol. Bioeng.* **111**, 1638–1647 (2014).
43. Uenaka, T. et al. Prevention of transgene silencing during human pluripotent stem cell differentiation. *Cell Stem Cell* **33**, 517–530 (2026).
44. Yanagi, T. et al. Termination sequence between an inducible promoter and ubiquitous chromatin opening element (UCOE) reduces gene expression leakage and silencing. *J. Biol. Eng.* **19**, 29 (2025).
45. Guichardaz, M., Bottini, S., Balmas, E. & Bertero, A. Overcoming the silencing of doxycycline-inducible promoters in hiPSC-derived cardiomyocytes. *Open Res. Eur.* **4**, 266 (2024).
46. Jillette, N., Du, M., Zhu, J. J., Cardoz, P. & Cheng, A. W. Split selectable markers. *Nat. Commun.* **10**, 4968 (2019).
47. Kelkar, A. et al. Doxycycline-dependent self-inactivation of CRISPR-Cas9 to temporally regulate on- and off-target editing. *Mol. Ther.* **28**, 29–41 (2020).
48. Ng, A. H. M. et al. A comprehensive library of human transcription factors for cell fate engineering. *Nat. Biotechnol.* **39**, 510–519 (2021).
49. Otomo, J., Woltjen, K. & Sakurai, H. Uniform transgene activation in Tet-On systems depends on sustained rtTA expression. *iScience* **26**, 107685 (2023).
50. Randolph, L. N., Bao, X., Zhou, C. & Lian, X. An all-in-one, Tet-On 3G inducible PiggyBac system for human pluripotent stem cells and derivatives. *Sci. Rep.* **7**, 1549 (2017).
51. Haenebalcke, L. et al. The ROSA26-iPSC mouse: a conditional, inducible, and exchangeable resource for studying cellular (de) differentiation. *Cell Rep.* **3**, 335–341 (2013).
52. Shin, S. W., Min, H., Kim, J. & Lee, J. S. A precise and sustainable doxycycline-inducible cell line development platform for reliable mammalian cell engineering with gain-of-function mutations. *Metab. Eng.* **86**, 12–28 (2024).
53. Rieck, S. et al. Forward programming of human induced pluripotent stem cells via the ETS variant transcription factor 2: rapid, reproducible, and cost-effective generation of highly enriched, functional endothelial cells. *Cardiovasc. Res.* **120**, 1472–1484 (2024).
54. Ding, Y. et al. ETV2 overexpression promotes efficient differentiation of pluripotent stem cells to endothelial cells. *Biotechnol. Bioeng.* **122**, 1914–1928 (2025).
55. Wang, N. B. et al. Compact transcription factor cassettes generate functional, engraftable motor neurons by direct conversion. *Cell Syst.* **16**, 101206 (2025).
56. Liu, Z. et al. Systematic comparison of 2A peptides for cloning multi-genes in a polycistronic vector. *Sci. Rep.* **7**, 2193 (2017).
57. Joung, J. et al. A transcription factor atlas of directed differentiation. *Cell* **186**, 209–229.e26 (2023).
58. Skylar-Scott, M. A. et al. Orthogonally induced differentiation of stem cells for the programmatic patterning of vascularized organoids and bioprinted tissues. *Nat. Biomed. Eng.* **6**, 449–462 (2022).
59. Karbassi, E. et al. Targeted CRISPR activation is functional in engineered human pluripotent stem cells but undergoes silencing after differentiation into cardiomyocytes and endothelium. *Cell. Mol. Life Sci.* **81**, 95 (2024).
60. Weber, E., Engler, C., Gruetzner, R., Werner, S. & Marillonnet, S. A modular cloning system for standardized assembly of multigene constructs. *PLoS ONE* **6**, e16765 (2011).
61. Kabaria, S. R. et al. Programmable promoter editing for precise control of transgene expression. *Nat. Biotechnol.* https://doi.org/10.1038/s41587-025-02854-y (2025).
62. Love, K. S., Johnstone, C. P., Peterman, E. L., Gaglione, S. & Galloway, K. E. Model-guided design of microRNA-based gene circuits supports precise dosage of transgenic cargoes into diverse primary cells. *Cell Syst.* **16**, 101269 (2025).
63. Hermann, M. et al. Binary recombinase systems for high-resolution conditional mutagenesis. *Nucleic Acids Res.* **42**, 3894–3907 (2014).
64. Hofbauer, P. et al. Cardioids reveal self-organizing principles of human cardiogenesis. *Cell* **184**, 3299–3317.e22 (2021).
65. Campostrini, G. et al. Generation, functional analysis and applications of isogenic three-dimensional self-aggregating cardiac microtissues from human pluripotent stem cells. *Nat. Protoc.* **16**, 2213–2256 (2021).
66. Chen, Y. et al. A versatile polypharmacology platform promotes cytoprotection and viability of human pluripotent and differentiated cells. *Nat. Methods* **18**, 528–541 (2021).
67. Wershof, E. et al. A FIJI macro for quantifying pattern in extracellular matrix. *Life Sci. Alliance* **4**, e202000880 (2021).
68. Blanch-Asensio, A. et al. STRAIGHT-IN Dual: a platform for dual single-copy integrations of DNA payloads and gene circuits into human induced pluripotent stem cells. *Zenodo* https://doi.org/10.5281/zenodo.17930642 (2026).

Acknowledgements

We thank N. Geijsen and P. Shang for providing TAT-Cre protein, the LUMC flow cytometry facility for sorting the cells and the Laboratory for Diagnostic Genome Analysis (LUMC) for karyotyping. This work was supported by the Netherlands Organ-on-Chip Initiative, a Gravitation project of the Nederlandse Organisatie voor Wetenschappelijk Onderzoek (NWO), funded by the Ministry of Education, Culture and Science of the government of the Netherlands (024.003.001); the NWO-funded LymphChip project (NWAORC 2019 1292.19.019) as part of the NWA research programme 'Research on Routes by Consortia (ORC)'; funding from the NWO Open Competition XS programme (OCENW.XS23.4.123); a ZonMw PSIDER consortium grant (10250022120002; GREAT); and a Marie Sklodowska-Curie fellowship (101152209) under the European Union's Horizon 2020 research and innovation programme. It also forms part of the project 'Innovative Stem Cell Technology Infrastructure for Human Organ and Disease Models', funded by the NWO Large-Scale Research Infrastructure programme (184.036.006). The Novo Nordisk Foundation Center for Stem Cell Medicine (reNEW) is supported by a Novo Nordisk Foundation grant (NNF21CC0073729). Additional support was provided by the National Institute of General Medical Sciences of the National Institutes of Health (R35-GM143033 to K.E.G.), the National Science Foundation under the NSF-CAREER award (2339986), and with funding from the Institute for Collaborative Biotechnologies (W911NF-19-2-0026), by the Air Force Research Laboratory MURI (FA9550-22-1-0316) and the Pershing Square Foundation MIND Prize. This study also received funding from the European Research Council (ERC) under the European Union's Horizon 2000 research and innovation programme (101042634). ChatGPT was used to help reduce the word count of the paper. All suggested revisions were reviewed and assessed by the authors.

Author contributions

A.B.-A. developed and optimized the protocols described in this paper, designed and performed the experiments, analysed the data and wrote the paper. D.S.P. developed and optimized some of the protocols described in this paper, designed and performed some of the experiments, contributed to drafting the paper and revised it for important intellectual content. S.C., B.B.J., M.R.M.B. and N.B.W. designed and performed some of the experiments, and contributed to drafting the paper. V.V.O. contributed intellectual content. A.A. analysed the data, contributed to drafting the paper and revised it for important intellectual content. C.L.M. acquired some of the funding and revised the paper for important intellectual content. K.E.G. and R.P.D. supervised the study, acquired some of the funding and revised the paper for important intellectual content. All authors approved the final paper.

Competing interests

C.L.M. is a co-founder of Pluriomics B.V. (now Ncardia B.V.) and has advisory roles in HeartBeat.bio AG, Angios GmBH, Mogrify Limited and Sartorius AG. R.P.D. declares research funding from Sartorius AG for an unrelated study. A.B.-A., D.S.P., S.C., B.B.J., M.R.M.B., N.B.W., V.V.O., A.A. and K.E.G. declare no competing interests.

Additional information

Extended data is available for this paper at https://doi.org/10.1038/s41551-026-01677-9.

Supplementary information The online version contains supplementary material available at https://doi.org/10.1038/s41551-026-01677-9.

Correspondence and requests for materials should be addressed to Kate E. Galloway or Richard P. Davis.

Peer review information *Nature Biomedical Engineering* thanks the anonymous reviewer(s) for their contribution to the peer review of this work. Peer reviewer reports are available.

https://doi.org/10.1038/s41551-026-01677-9

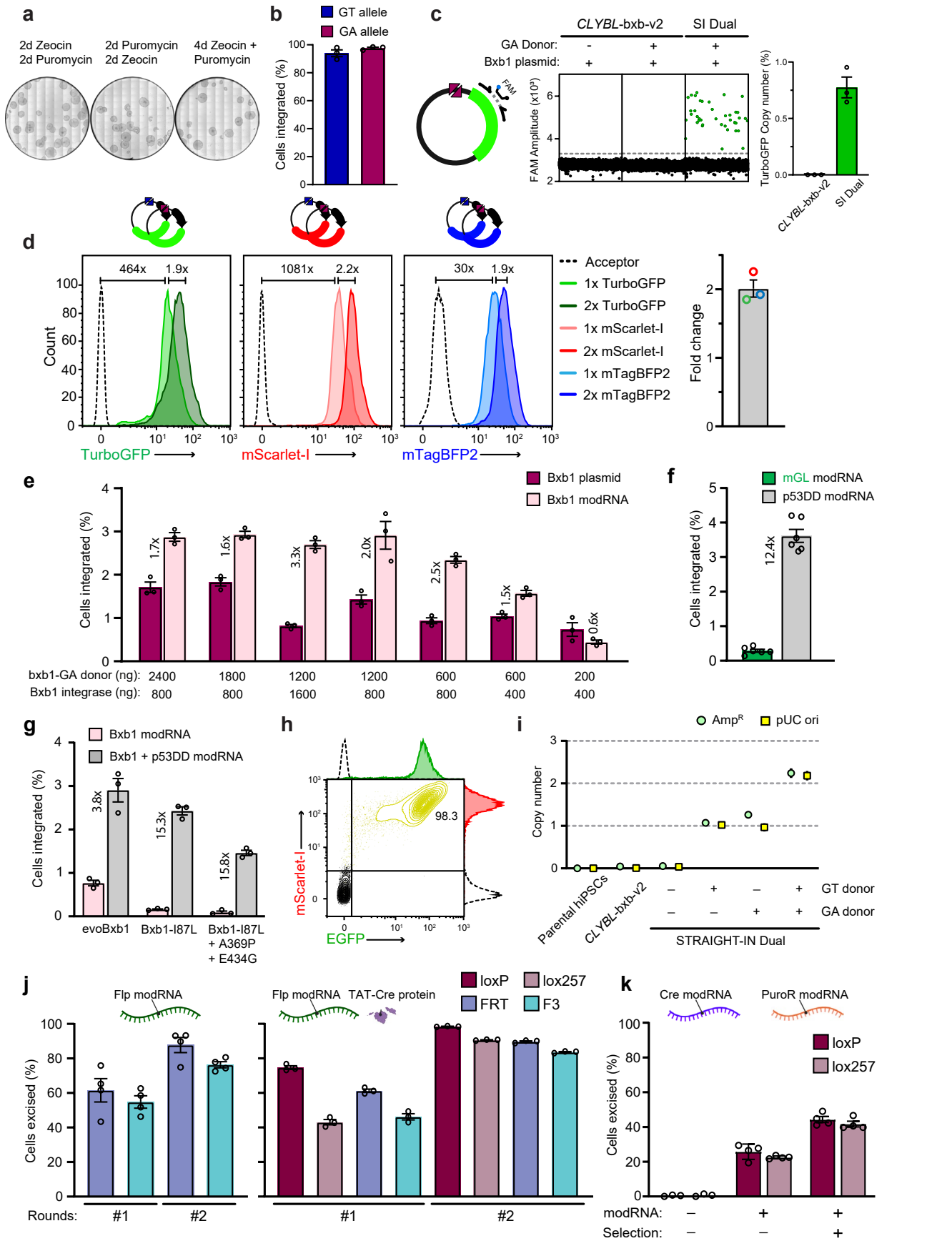

Extended Data Fig. 1 | See next page for caption.

https://doi.org/10.1038/s41551-026-01677-9

Extended Data Fig. 1 | Optimizing the integration and excision processes in STRAIGHT-IN Dual hiPSCs. (a) Alkaline phosphatase staining of hiPSCs following sequential or simultaneous antibiotic selection to enrich for cells with both GT and GA donor plasmid integrations. **(b)** Mean integration efficiencies of GT and GA donor plasmids co-delivered and selected simultaneously. N = 3 independent transfections; error bars, ±SEM. **(c)** GA-TurboGFP donor plasmid schematic (*left*) and representative ddPCR dot plots confirming GA donor integration in STRAIGHT-IN Dual hiPSCs (*middle*). Green dots represent droplets containing the indicated donor sequence. Mean percentages of hiPSCs positive for the *TurboGFP* sequence (*right*). N = 3 independent transfections; error bars, ±SEM. **(d)** Flow cytometry analysis of STRAIGHT-IN Dual hiPSCs carrying one (1x) or two (2x) integrated fluorescent reporter payloads, as indicated. Dashed line indicates untransfected STRAIGHT-IN Dual hiPSCs. Fold change was calculated as the G-mean ratio. *Right*, mean fold change for 2x versus 1x integration. reporters. N = 3 independent transfections; error bars, ±SEM. **(e)** Mean (pre-selection) integration efficiency of a GA donor plasmid co-transfected with Bxb1 expression plasmid or *Bxb1* modRNA (input amounts as indicated). N = 3 independent transfections; error bars, ±SEM. **(f)** Mean (pre-selection) integration efficiency of a GA donor plasmid co-transfected with Bxb1 expression plasmid and either *mGreenLantern* (*mGL*) or *p53DD* modRNA. N = 6 independent transfections; error bars, ±SEM. **(g)** Mean (pre-selection) integration efficiency of a GA donor plasmid co-transfected with the indicated *Bxb1* modRNA, with or without *p53DD* modRNA. N = 3 independent transfections; error bars, ±SEM. **(h)** Flow cytometry analysis 6 days after co-transfection of GT and GA donor plasmids encoding *mScarlet-I* and *EGFP*, respectively, together with *Bxb1* and *p53DD* modRNAs, followed by 3 days of antibiotic selection. Dashed line indicates untransfected hiPSCs. **(i)** ddPCR-based quantification of AmpR and pUC ori backbone copy number following integration and selection with GT and/or GA donor plasmids. Symbols show the estimated copy-number; error bars indicate the Poisson 95% confidence interval. Data are from a representative transfection (N = 1 biological replicate). **(j)** Mean excision efficiency of the indicated flanking regions measured by ddPCR following *Flp* modRNA alone (*left*), or co-delivery of TAT-Cre and *Flp* modRNA (*right*). Recombinases were delivered once (#1) or twice (#2). N = 3 independent transfections; error bars ±SEM. **(k)** Mean excision efficiency of the indicated flanking regions measured by ddPCR following co-transfection of *Cre* and *PuroR* modRNAs, with (+) or without (-) 24 h puromycin selection. N = 4 independent transfections; error bars ±SEM. Schematics in **c**,**d**, **j** and **k** created in BioRender; Blanch Asensio, A. https://biorender.com/i96jbul (2026).

https://doi.org/10.1038/s41551-026-01677-9

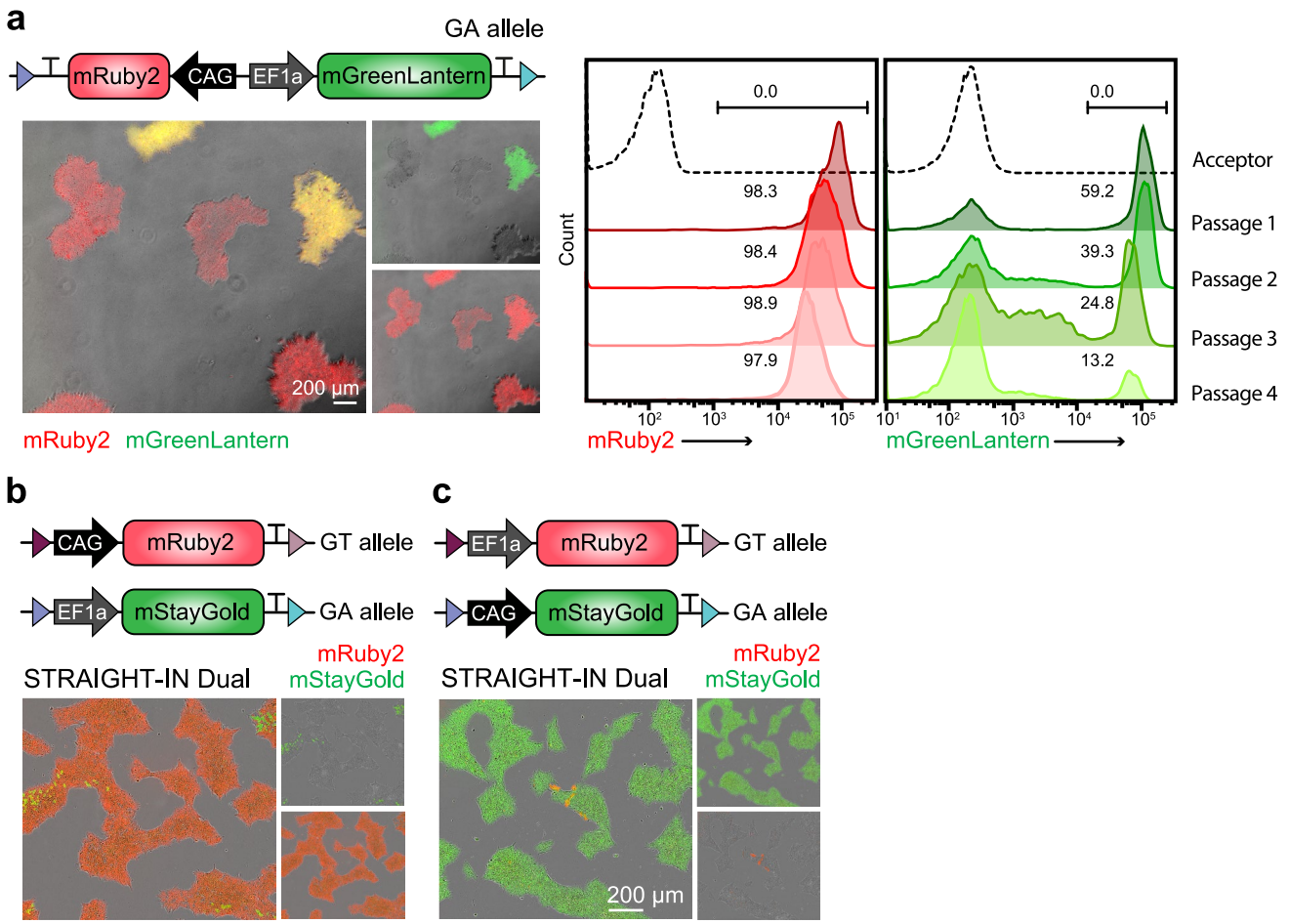

Extended Data Fig. 2 | Transgenes driven by the hEF1a promoter are silenced in hiPSCs over time. (a) Representative overlaid fluorescence and phase contrast images (*left*), and flow cytometry analysis over 4 passages (*right*), of hiPSCs expressing mRuby2 and mGreenLantern reporters in cis, driven by the CAG and hEF1a promoters respectively, and integrated at the GA allele. Dashed lines represent untransfected hiPSCs. **(b)** Overlaid fluorescence and phase contrast images (*left*), and flow cytometric analysis (*right*), of hiPSCs expressing mRuby2 and mStayGold reporters in trans, driven by the CAG and hEF1a promoters respectively, and integrated in the GT and GA alleles. Dashed lines represent untransfected hiPSCs. **(c)** Overlaid fluorescence and phase contrast images of hiPSCs expressing mRuby2 and mStayGold reporters in trans, driven by the hEF1a and CAG promoters respectively, and integrated in the GT and GA alleles.

https://doi.org/10.1038/s41551-026-01677-9

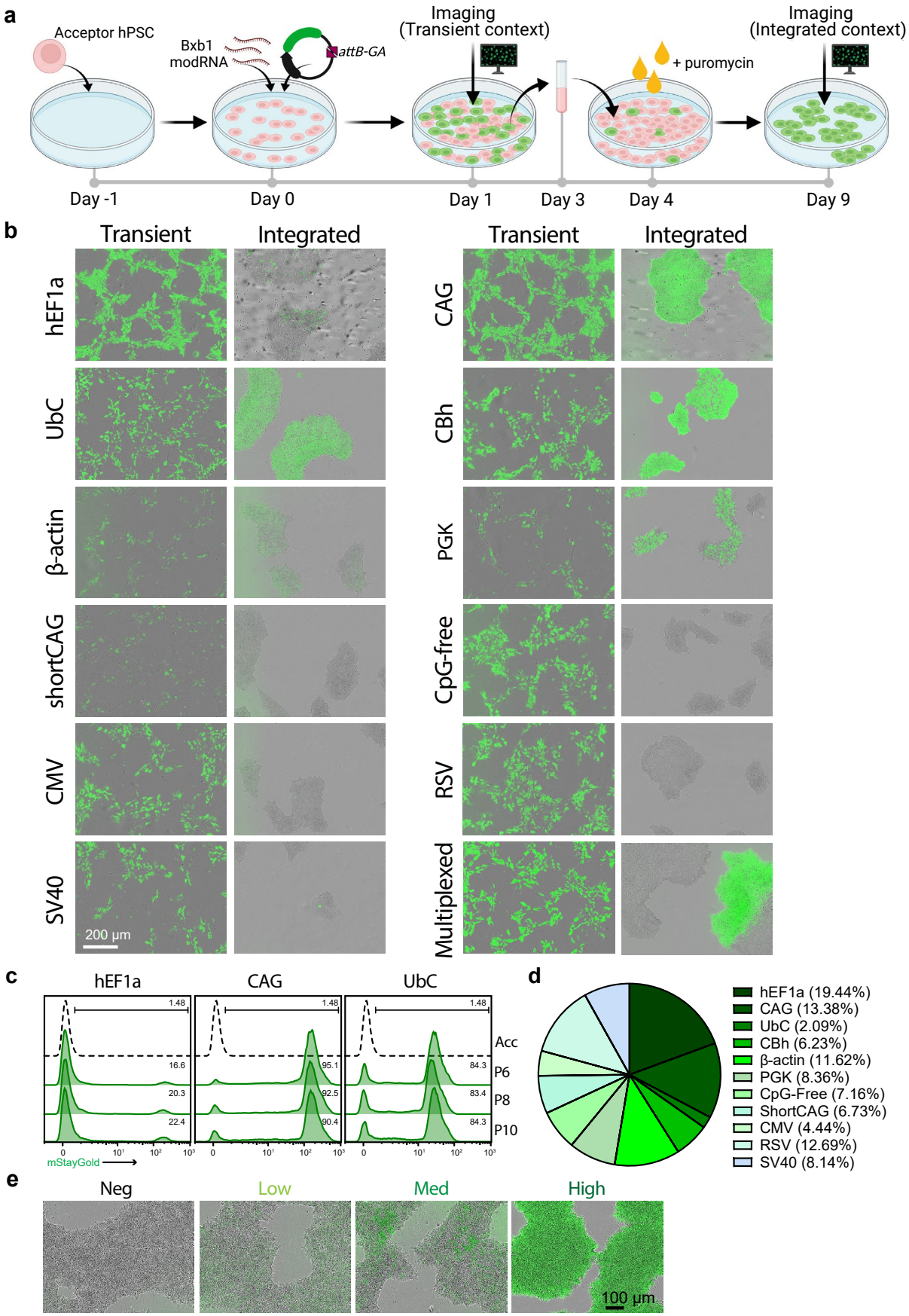

Extended Data Fig. 3 | See next page for caption.

https://doi.org/10.1038/s41551-026-01677-9

Extended Data Fig. 3 | Comparison of transient and integrated promoter-driven transgene expression in hiPSCs. (a) Schematic illustrating the experimental design. STRAIGHT-IN Dual hiPSCs were transfected with *Bxb1* modRNA and GA donor plasmids encoding *mStayGold* under the control of diverse promoter sequences. Fluorescence was assessed 24 h post-transfection (transient expression) and again following puromycin selection and replating (genomic integrated expression). **(b)** Representative fluorescence/phase-contrast images of hiPSCs expressing mStayGold driven under control of the indicated promoters, comparing transient and integrated expression. **(c)** Flow cytometry analysis of mStayGold expression over 10 passages in hiPSCs with integrated constructs driven by hEF1a, CAG or UbC promoters. **(d)** Pie chart of bulk population showing the percentage of sequencing reads corresponding to each of the 11 integrated promoter constructs in the pooled bulk population. **(e)** Representative fluorescence/phase-contrast images of sorted bulk populations based on mStayGold expression levels (negative (neg), low, medium (med), and high), corresponding to the clusters shown in Fig. 3d. Schematic in **a** created in BioRender; Blanch Asensio, A. https://biorender.com/zsi23qj (2026).

https://doi.org/10.1038/s41551-026-01677-9

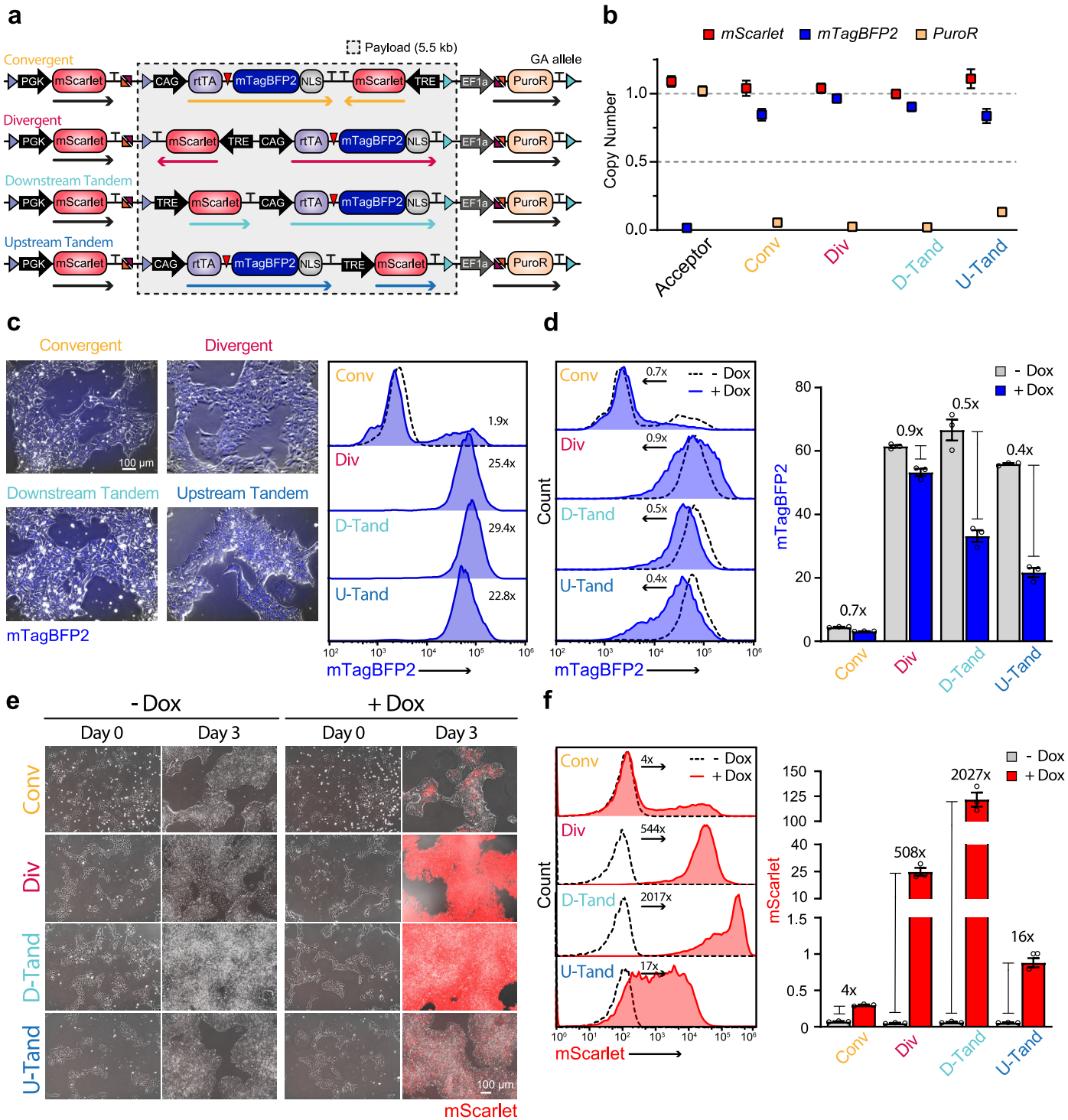

Extended Data Fig. 4 | Evaluation of gene syntax configurations in an all-in-one Tet-On 3G inducible system. (a) Schematic of the four cis-configured Tet-On 3G constructs, showing the orientation and order of the inducible (TRE-*mScarlet*) and constitutive (CAG-*rtTA-T2A-mTagBFP2*) cassettes, along with the upstream and downstream auxiliary elements. The grey-shaded region indicates the genomic sequence retained following Flp-mediated excision. **(b)** ddPCR analysis confirming single-copy integration of *mScarlet* and *mTagBFP2*, and the absence of *PuroR* following excision. Symbols show the estimated copy-number; error bars indicate the Poisson 95% confidence interval. Data are from a representative transfection (N = 1 biological replicate). **(c)** Representative fluorescence/phase-contrast images (*left*) and flow cytometry analysis (*right*) of hiPSCs constitutively expressing mTagBFP2 from the constructs in (**a**) prior to excision. Fold change was calculated by comparing the G-mean relative to untransfected hiPSCs (dashed line), with values shown in plots. **(d)** Flow cytometry analysis of mTagBFP2 expression in the absence (dashed line) or presence (blue) of doxycycline for 3 days (*left*), and quantification of G-mean fluorescence values (*right*). Fold change values (x) are calculated relative to untreated samples. N = 3 biological replicates; mean ± SEM. **(e)** Representative fluorescence/phase-contrast images of hiPSCs expressing inducible mScarlet from the constructs in (**a**) in the absence or presence of doxycycline for 3 days. **(f)** Flow cytometry analysis of mScarlet expression in the absence (dashed line) or presence (red) of doxycycline for 3 days (*left*), and quantification of G-mean fluorescence values (*right*). Fold change values (x) are calculated relative to untreated samples. N = 3 biological replicates; mean ± SEM.

https://doi.org/10.1038/s41551-026-01677-9

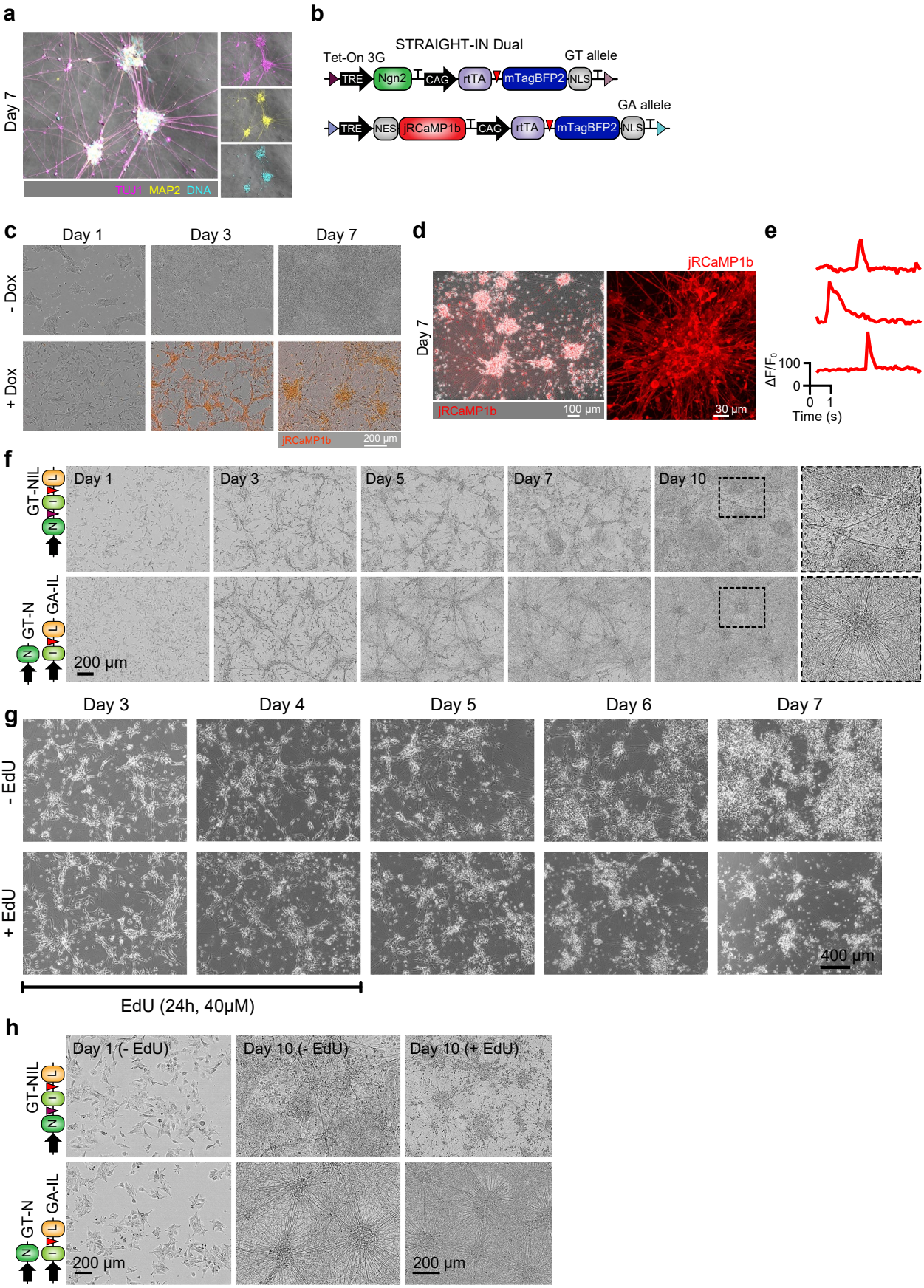

Extended Data Fig. 5 | See next page for caption.

https://doi.org/10.1038/s41551-026-01677-9

Extended Data Fig. 5 | Forward programming of hiPSCs to neurons or motor neurons using the Tet-On 3G system with downstream tandem orientation. **(a)** Overlaid immunofluorescence and phase contrast images showing TUJ1 (magenta) MAP2 (yellow), and DNA (cyan) in cells cultured with doxycycline for 7 days. **(b)** Schematic of STRAIGHT-IN Dual hiPSCs with the inducible *Ngn2* cassette in the GT allele, and a similar downstream tandem construct containing *jRCaMP1b* in the GA allele. **(c)** Representative fluorescence/phase-contrast images of cells cultured in the presence or absence of doxycycline for the indicated time points. **(d)** Representative fluorescence/phase-contrast (*left*) and jRCaMP1b fluorescence (*right*) images of forward programmed iNs at day 7. **(e)** Representative jRCaMP1b fluorescence traces showing cytosolic Ca^{2+} transients from forward programmed iNs. **(f)** Phase contrast images of GT-NIL and GT-N + GA-IL cells over 10 days of culture in the presence of doxycycline. **(g)** Phase contrast images of GT-NIL cells at different time points cultured with or without EdU administered for 48 h between days 3–5. **(h)** Phase contrast images of GT-NIL and GT-N + GA-IL cells containing the indicated transcription factor cassettes for motor neuron induction at day 1 and 10 of treatment with doxycycline ± EdU for 48 h.

https://doi.org/10.1038/s41551-026-01677-9

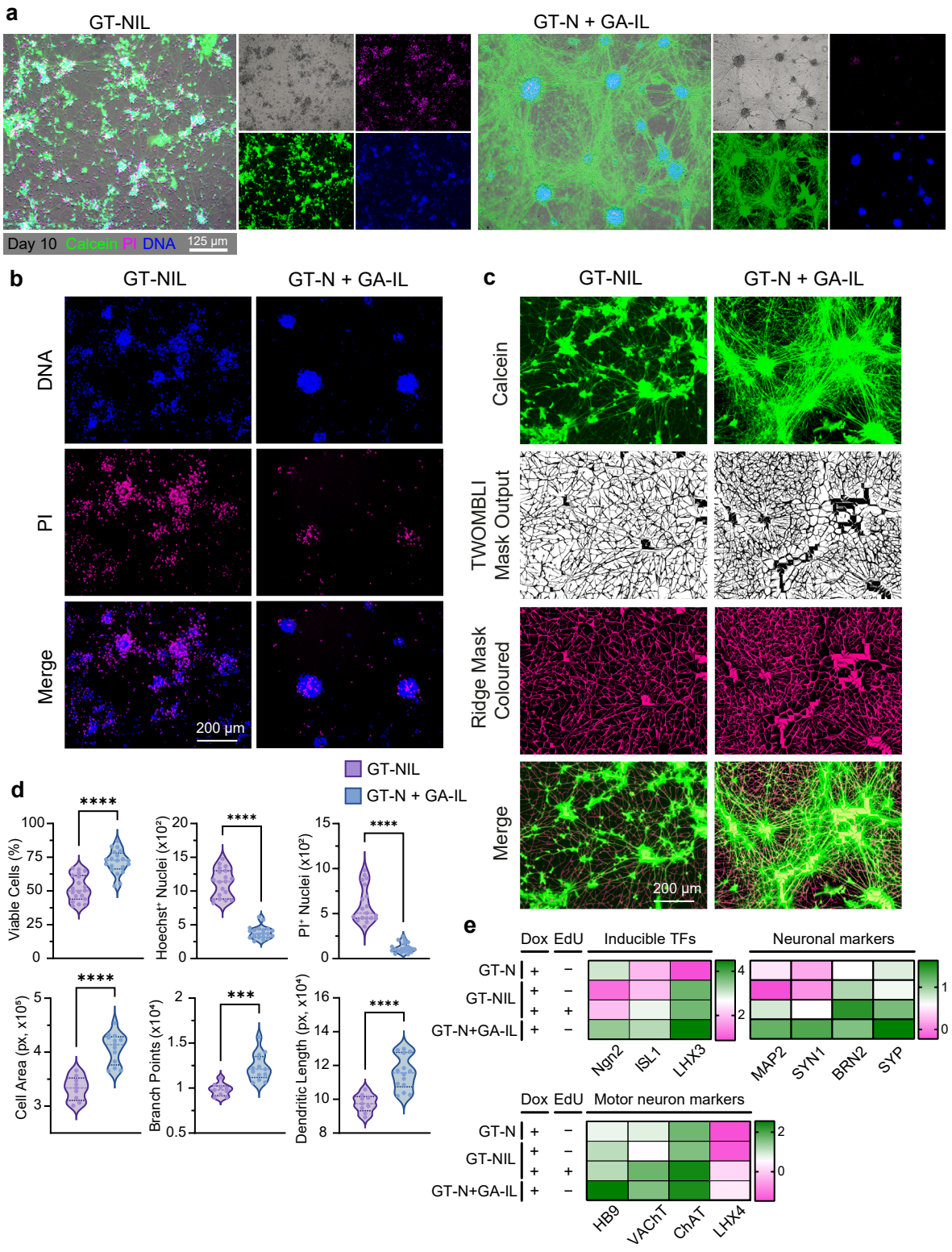

Extended Data Fig. 6 | See next page for caption.

https://doi.org/10.1038/s41551-026-01677-9

Extended Data Fig. 6 | Characterization of iMNs generated from GT-NIL and GT-N + GA-IL hiPSC lines. (a) Fluorescence/phase-contrast images on day 10 of doxycycline induction showing staining for live cells (Calcein AM, green), dead cells (propidium iodide, magenta) and DNA (Hoechst, blue). **(b)** Representative fluorescence images of Hoechst-stained nuclei to visualize DNA, and propidium iodide $(PI)^+$ non-viable cells. **(c)** Representative fluorescence images of Calcein AM-stained live cells and quantified mask output of the mapped ridgelines. **(d)** Violin plots quantifying iMN viability and morphology for the indicated single- and dual-cassette configurations from images acquired as in **b** and **c**. Metrics include the percentage of viable iMNs, counts of $Hoechst^+$ nuclei and PI^+ nuclei, cell area, number of branch points and dendritic length. Violin width represents the kernel density (data distribution). The center line indicates the median, and the outer dotted lines indicate the 25th and 75th percentiles. For Hoechst and propidium iodide (PI) staining, 3–4 images were analyzed per differentiation (technical replicates) across five independent differentiations (biological replicates). For Calcein AM staining, 3–5 images were analyzed per differentiation (technical replicates) across 3 independent differentiations (biological replicates). ***, $P \leq 0.001$; ****, $P \leq 0.0001$ (unpaired two-tailed t test). Exact P values are ≤0.0001. **(e)** Gene expression analysis of inducible transcription factors, neuronal markers, and motor neuron markers in cells containing the GT-N, GT-NIL, and GT-N + GA-IL constructs, cultured with doxycycline for 10 days. Values are normalized to *RPL37A* and shown relative to uninduced conditions (log_{10}-transformed). N = 3 independent differentiations.

https://doi.org/10.1038/s41551-026-01677-9

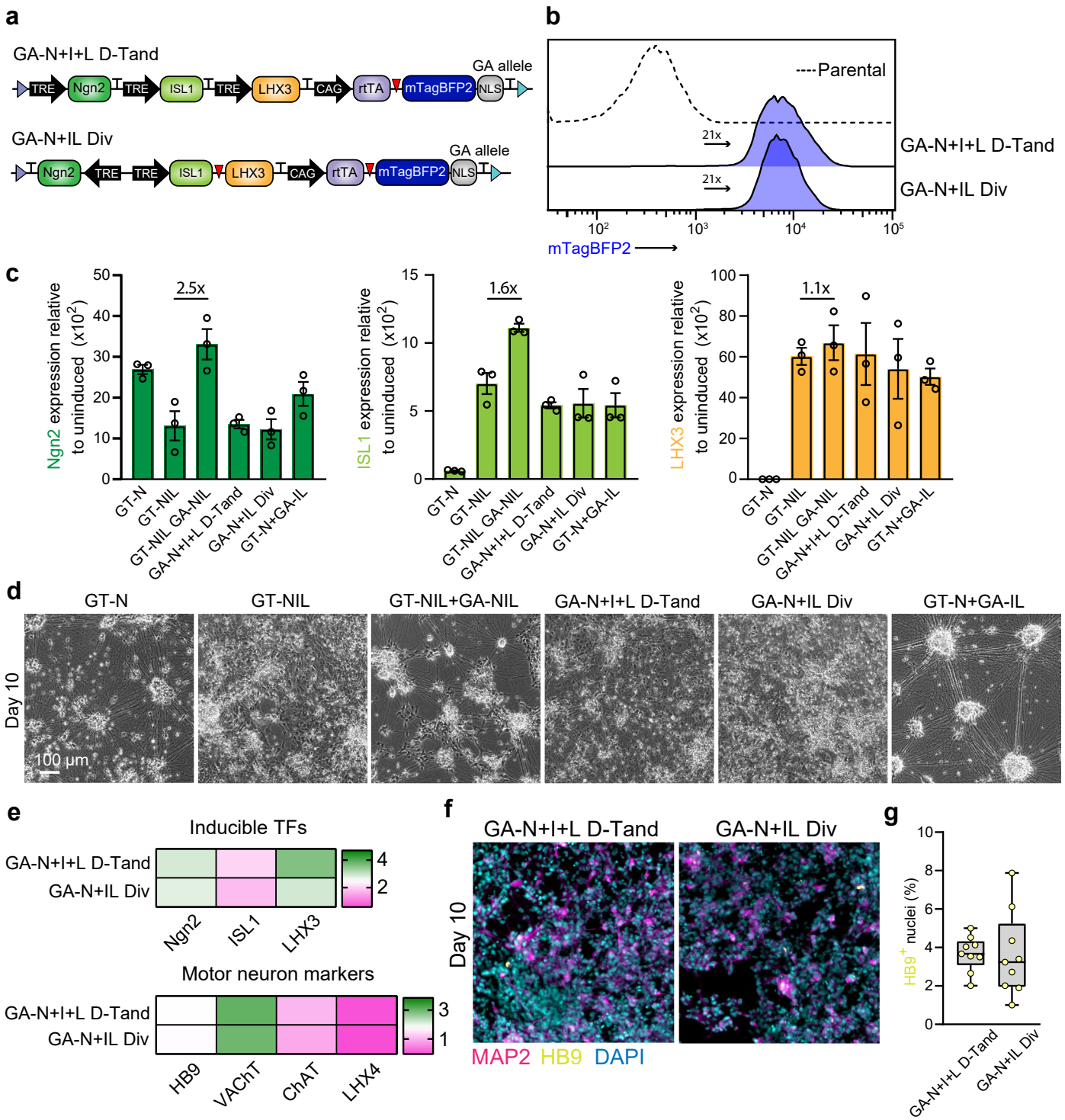

Extended Data Fig. 7 | Characterization of iMNs generated from GT-NIL, GT-NIL + GA-NIL, GA-N + I + L D-Tand, GA-N + IL Div and GT-N + GA-IL hiPSC lines. (a) Schematic of STRAIGHT-IN single hiPSCs with the indicated constructs integrated in the GA allele. **(b)** Flow cytometry analysis of mTagBFP2 expression in hiPSC lines with the indicated cassettes from panel (**a**) integrated in the GA allele, and quantification of G-mean fluorescence values. Fold change values (x) are calculated relative to the untransfected parental hiPSC line. **(c)** Bar graph of expression analysis of inducible transcription factors in cells containing the indicated constructs, cultured with doxycycline for 3 days. Values are normalized to *RPL37A* and shown relative to uninduced conditions (log_{10}-transformed). N = 3 independent differentiations; error bars, ±SEM. **(d)** Phase contrast images of cells containing the indicated constructs after 10 days of culture in the presence of doxycycline. **(e)** Gene expression analysis of inducible transcription factors and motor neuron markers in cells containing the GA-N + I + L D-Tand and GA-N + IL Div constructs and cultured with doxycycline for 10 days. Values are normalized to *RPL37A* and shown relative to uninduced conditions (log_{10}-transformed). N = 3 independent differentiations. **(f)** Immunofluorescence images (MAP2, magenta; HB9, yellow; DNA, cyan) of GA-N + I + L D-Tand and GA-N + IL Div cells treated with doxycycline for 10 days. **(g)** Box-and-whisker plots showing percentage of $HB9^+$ nuclei relative to $DAPI^+$ nuclei from images acquired as in (**f**). The center line indicates the median (50th percentile). The lower and upper bounds of the box indicate the 25th and 75th percentiles, and whiskers extend to the minimum and maximum values. For each condition, 2–3 images (technical replicates) were analyzed per differentiation across 3 independent differentiations (biological replicates).

https://doi.org/10.1038/s41551-026-01677-9

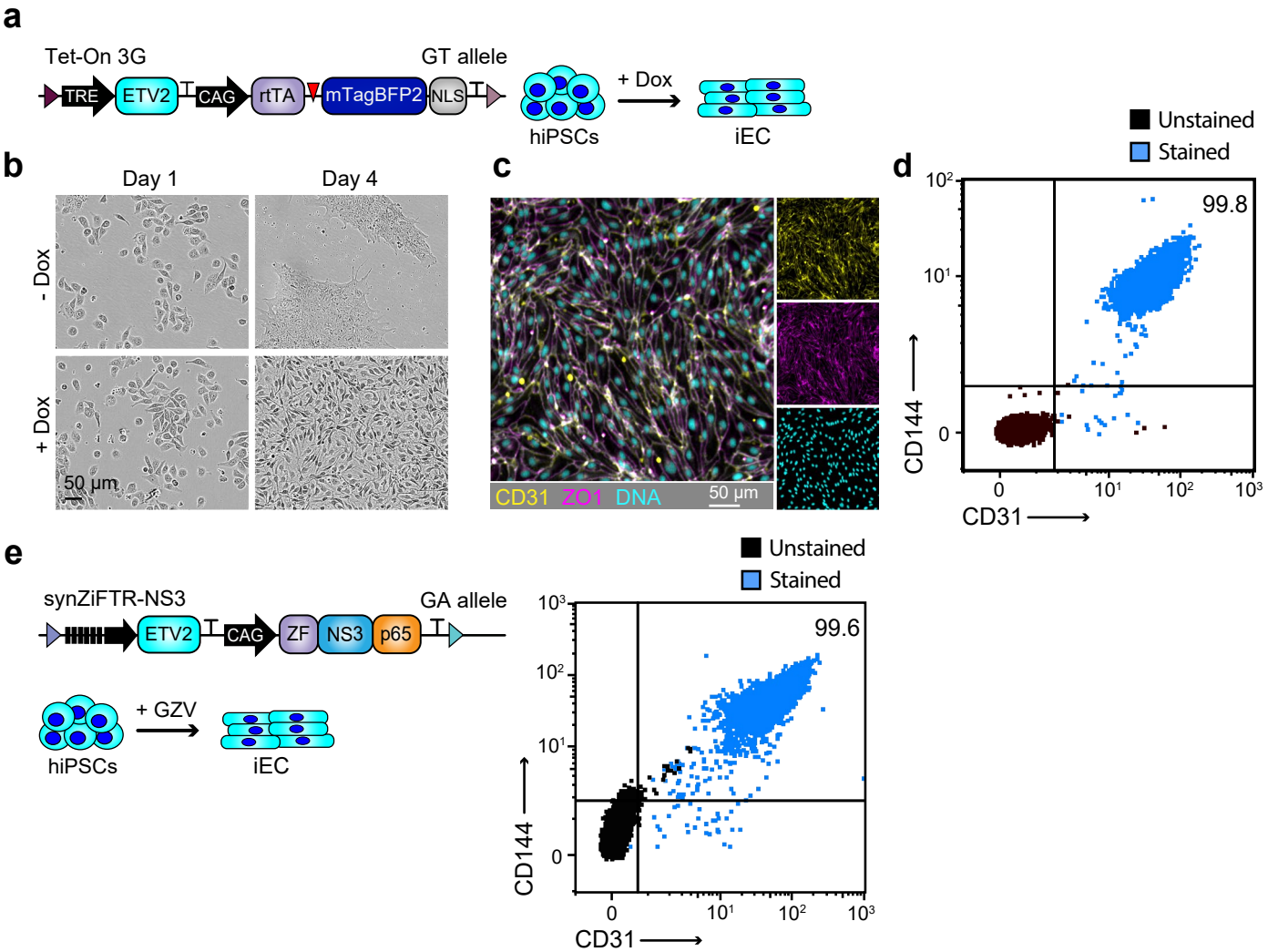

Extended Data Fig. 8 | Characterization of iECs following *ETV2* overexpression using the Tet-On 3G system. (**a**) Schematic of the downstream tandem configuration for a doxycycline-inducible *ETV2* expression cassette. (**b**) Phase contrast images showing cell morphology at the indicated time points in the absence (-) or presence (+) of doxycycline. (**c**) Immunofluorescence images of cells cultured with doxycycline for 4 days and stained for CD31 (yellow), ZO1 (magenta), and DNA (cyan). **(d, e)** Flow cytometry analysis of endothelial markers CD144 (VE-cadherin) and CD31 (PECAM-1) on day 4 of *ETV2* induction using either the all-in-one Tet-On 3G (**d**) or synZiFTR-NS3 (**e**) inducible system. The iECs in (**e**) are derived from the dual-fate hiPSC line shown in Fig. 6e, f.

https://doi.org/10.1038/s41551-026-01677-9

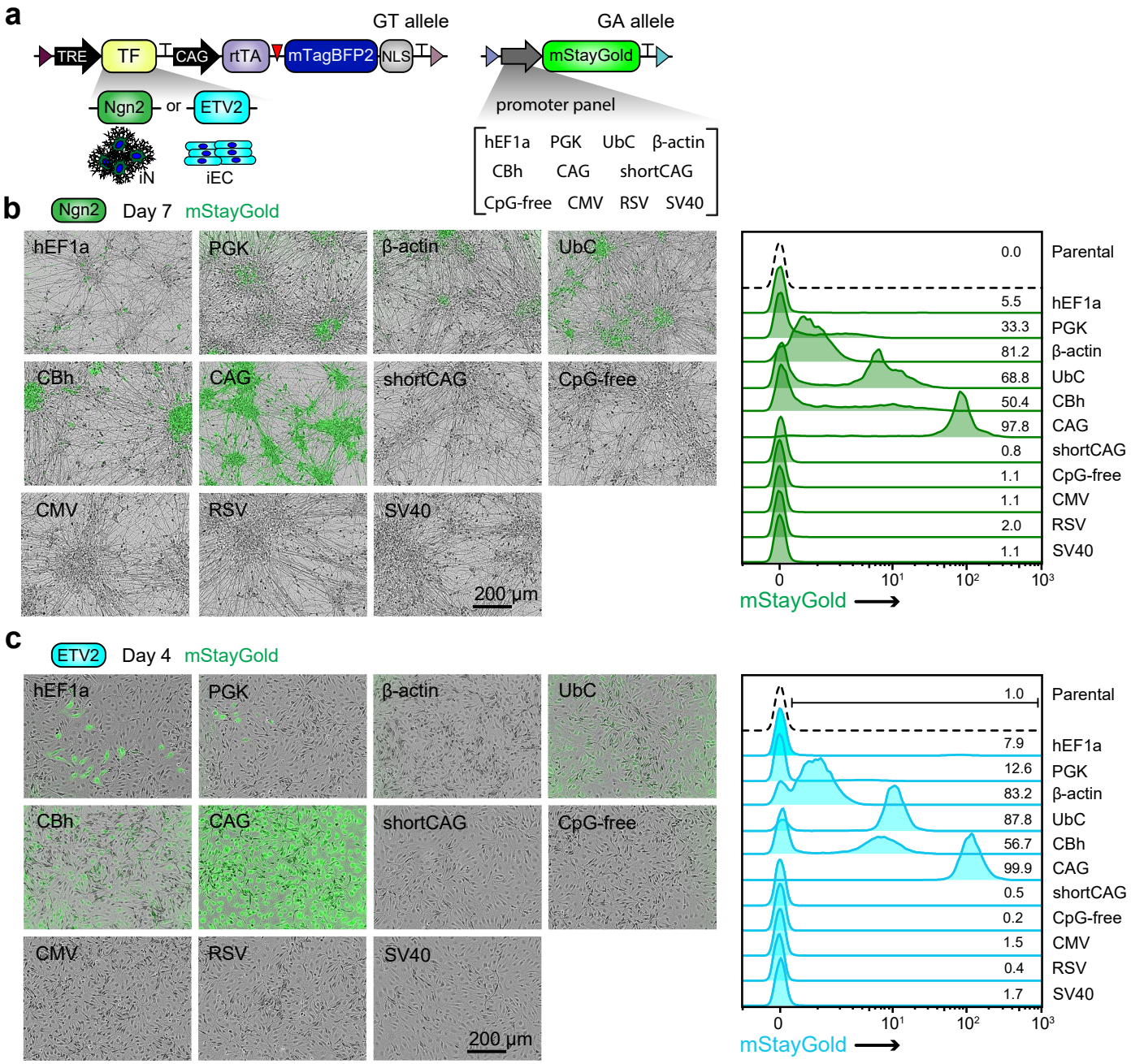

Extended Data Fig. 9 | Evaluation of promoter activity in iNs and iECs using STRAIGHT-IN Dual. (**a**) Schematic of the downstream tandem configuration for a doxycycline-inducible *Ngn2* or *ETV2* cassette integrated in the GT allele (*left*), and a schematic of the promoter panel driving mStayGold reporter expression integrated in the GA allele (*right*) of the *CLYBL* locus. (**b, c**) Overlaid fluorescence and phase contrast images (*left*) and flow cytometry analysis of mStayGold expression (*right*) in cells cultured with doxycycline for 7 (**b**; *Ngn2*) or 4 days (**c**; *ETV2*). The promoter sequences assessed are indicated.

https://doi.org/10.1038/s41551-026-01677-9

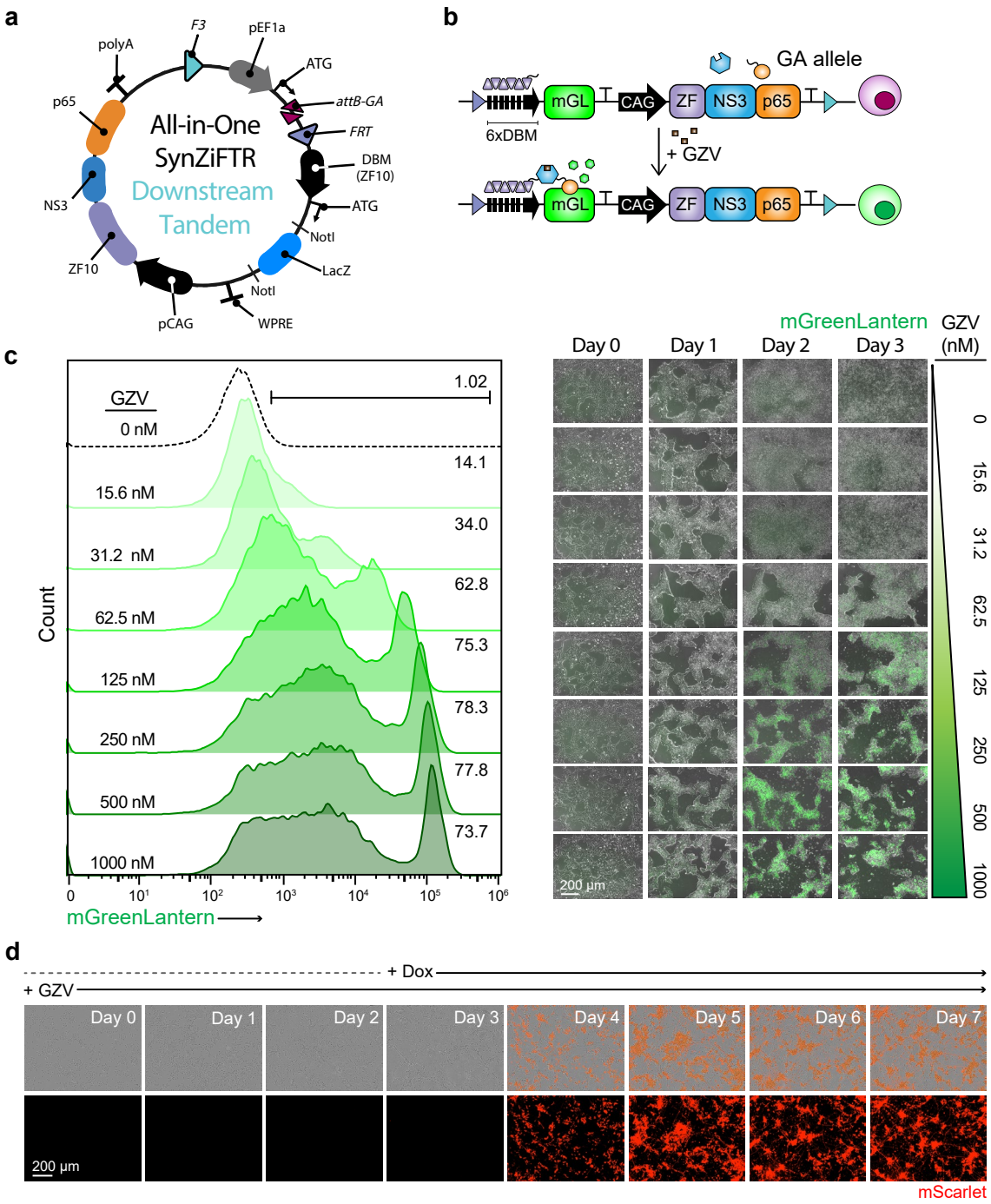

Extended Data Fig. 10 | Transgene overexpression in hiPSCs using the GZV-inducible synZiFTR system. (a) Schematic of the downstream tandem all-in-one grazoprevir-inducible synZiFTR GA donor plasmid, in which the *LacZ* cassette is replaced with the gene of interest (GOI) via NotI digestion and isothermal assembly. **(b)** Schematic of a downstream tandem synZiFTR cassette driving grazoprevir-inducible *mGreenLantern* expression, integrated in the GA allele. **(c)** Flow cytometry analysis (*left*) and overlaid fluorescence and phase-contrast images (*right*) of hiPSCs containing the construct shown in (**b**) and cultured in the absence (dashed line) or presence (green) of increasing GZV concentrations over a 3-day period. Values in the plot indicate the percentage of cells expressing mGreenLantern. **(d)** Timelapse fluorescence/phase-contrast images showing mScarlet expression in STRAIGHT-IN Dual hiPSCs containing the constructs shown in Fig. 6c. Cells were cultured for 7 days with grazoprevir added from day 0 and doxycycline from day 3. Schematic in **a** created in BioRender; Blanch Asensio, A. https://biorender.com/1ttbis5 (2026).

nature portfolio

Corresponding author(s): Kate E. Galloway
Richard P. Davis

Last updated by author(s): Feb 12, 2026

Reporting Summary

Nature Portfolio wishes to improve the reproducibility of the work that we publish. This form provides structure for consistency and transparency in reporting. For further information on Nature Portfolio policies, see our Editorial Policies and the Editorial Policy Checklist.

Statistics

For all statistical analyses, confirm that the following items are present in the figure legend, table legend, main text, or Methods section.

n/a	Confirmed	
☐	☒	The exact sample size (*n*) for each experimental group/condition, given as a discrete number and unit of measurement
☐	☒	A statement on whether measurements were taken from distinct samples or whether the same sample was measured repeatedly
☐	☒	The statistical test(s) used AND whether they are one- or two-sided *Only common tests should be described solely by name; describe more complex techniques in the Methods section.*
☐	☒	A description of all covariates tested
☒	☐	A description of any assumptions or corrections, such as tests of normality and adjustment for multiple comparisons
☐	☒	A full description of the statistical parameters including central tendency (e.g. means) or other basic estimates (e.g. regression coefficient) AND variation (e.g. standard deviation) or associated estimates of uncertainty (e.g. confidence intervals)
☐	☒	For null hypothesis testing, the test statistic (e.g. *F*, *t*, *r*) with confidence intervals, effect sizes, degrees of freedom and *P* value noted *Give P values as exact values whenever suitable.*
☒	☐	For Bayesian analysis, information on the choice of priors and Markov chain Monte Carlo settings
☒	☐	For hierarchical and complex designs, identification of the appropriate level for tests and full reporting of outcomes
☒	☐	Estimates of effect sizes (e.g. Cohen's *d*, Pearson's *r*), indicating how they were calculated

Our web collection on statistics for biologists contains articles on many of the points above.

Software and code

Policy information about availability of computer code

Data collection	ImageJ (using TWOMBLI plugin) and CellProfiler (version 4.2.8).
Data analysis	Microsoft® Excel® for Microsoft 365 (Version 2308), GraphPad Prism (version 10.6.1) and BWA-MEM (version 0.7.17).

For manuscripts utilizing custom algorithms or software that are central to the research but not yet described in published literature, software must be made available to editors and reviewers. We strongly encourage code deposition in a community repository (e.g. GitHub). See the Nature Portfolio guidelines for submitting code & software for further information.

Data

Policy information about availability of data

All manuscripts must include a data availability statement. This statement should provide the following information, where applicable:

- Accession codes, unique identifiers, or web links for publicly available datasets
- A description of any restrictions on data availability
- For clinical datasets or third party data, please ensure that the statement adheres to our policy

DNA sequencing data was generated in this study. All relevant data have been deposited into the public repository European Nucleotide Archive (ENA), and can be accessed under accession code PRJEB108223. Data associated with this manuscript have been deposited in Zenodo at https://zenodo.org/records/17930642 including code for CellProfiler and NGS analysis. Source data are included with this paper. All plasmids and their sequences have been deposited on Addgene.

Research involving human participants, their data, or biological material

Policy information about studies with human participants or human data. See also policy information about sex, gender (identity/presentation), and sexual orientation and race, ethnicity and racism.

Reporting on sex and gender	This study did not involve human research participants. This study involved one female hiPSC line (LUMCi004-A-2; RRID:CVCL_C6UD). Features regarding the human pluripotent stem cell line are summarized in the Materials and Methods section under the "hiPSC line culture, subcloning and transfection" subheading. No active enrollment of donors was performed in this study
Reporting on race, ethnicity, or other socially relevant groupings	Not applicable
Population characteristics	Not applicable
Recruitment	Not applicable
Ethics oversight	Protocols for research involving human subjects and stem cell research were approved by the medical ethical committee at Leiden University Medical Center, the Netherlands (approval number P13.080).

Note that full information on the approval of the study protocol must also be provided in the manuscript.

Field-specific reporting

Please select the one below that is the best fit for your research. If you are not sure, read the appropriate sections before making your selection.

☒ Life sciences ☐ Behavioural & social sciences ☐ Ecological, evolutionary & environmental sciences

For a reference copy of the document with all sections, see nature.com/documents/nr-reporting-summary-flat.pdf

Life sciences study design

All studies must disclose on these points even when the disclosure is negative.

Sample size	Sample size was not predetermined using any specific method. Instead, at least three independent transfections, induction experiments and forward programming differentiations were performed.
Data exclusions	Not applicable
Replication	Plasmid transfection: Number of independent plasmid transfections are stated in the figure legends, with at least three independent plasmid transfections being performed. In all instances hiPSCs were harvested for gDNA extraction 3-4 days post transfection and used as independent samples for ddPCR analysis. Evaluation of transgene silencing: All individual hiPSC lines containing different promoter sequences as well as the pooled condition were monitored and assessed by flow cytometry for at least 4 passages. Doxycycline induction: Uninduced and induced data was collected from three independent inductions of 1 µM doxycycline for 3 days. Fold change measurements were calculated by dividing the geometric mean fluorescent intensity (mScarlet and mTagBFP2) of the induced condition and the uninduced condition. Grazoprevir induction: Uninduced and induced data was collected from one induction varying the grazoprevir concentration from 15.65 to 1000 nM for 3 days (Extended Figure 10). RT-qPCR analysis: The RNA was extracted using the same RNA extraction protocol from three independent differentiation batches for each cell type (hiPSC-derived neurons, motor neurons or endothelial cells). The differentiation procedure as well as the RNA extraction, cDNA synthesis and RT-qPCR is explained in the Materials and Methods section. Primer pairs used are listed in Supplementary Table 4.
Randomization	Samples were not randomly allocated because the study did not involve experimental group assignment. All samples were processed according to predefined, objective criteria inherent to the experimental design, and no covariates required balancing or control through randomization.
Blinding	Blinding was not relevant to this study because no subjective assessments or group-dependent interventions were performed during data collection or analysis. All measurements were generated through automated or standardized analytical pipelines that do not permit investigator influence.

Reporting for specific materials, systems and methods

We require information from authors about some types of materials, experimental systems and methods used in many studies. Here, indicate whether each material, system or method listed is relevant to your study. If you are not sure if a list item applies to your research, read the appropriate section before selecting a response.

Materials & experimental systems

n/a	Involved in the study
☐	☒ Antibodies
☐	☒ Eukaryotic cell lines
☒	☐ Palaeontology and archaeology
☒	☐ Animals and other organisms
☒	☐ Clinical data
☒	☐ Dual use research of concern
☒	☐ Plants

Methods

n/a	Involved in the study
☒	☐ ChIP-seq
☐	☒ Flow cytometry
☒	☐ MRI-based neuroimaging

Antibodies

Antibodies used

OCT3/4-BV421 BD Biosciences Cat#565644; RRID:AB_2739320 (1:50 dilution)
NANOG-PE BD Biosciences Cat#560483; RRID:AB_1645522 (1:50 dilution)
SSEA4-FITC BD Biosciences Cat#560126; RRID:AB_1645491 (1:50 dilution)
Tubulin beta 3 Biolegend Cat#801201; RRID:AB_2313773 (1:500 dilution)
MAP2 Cell Signaling Technology Cat#4542; RRID:AB_10693782 (1:500 dilution)
Alexa Fluor® 647 AffiniPure™ Donkey Anti-Goat IgG Jackson Immunoresearch Cat#705-605-147; RRID:AB_2340437 (1:500 dilution)
Alexa Fluor® 647 donkey anti-mouse IgG; RRID:AB_162542 ThermoFisher Cat#A-31571 (1:500 dilution)
Alexa Fluor® 555 rabbit anti-human FOXA2 Cell Signaling Technology #50079 (1:500 dilution)
Alexa Fluor® 647 rabbit anti-human GATA4 Cell Signaling Technology Cat#66309; RRID:AB_3697603 (1:200 dilution)
Alexa Fluor® 488 mouse anti-human Nestin Cell Signaling Technology Cat#35884; RRID:AB_3665833 (1:200 dilution)
Alexa Fluor® 647 rabbit anti-human PAX6 Cell Signaling Technology Cat#60433 (1:200 dilution)
Alexa Fluor® 488 rabbit anti-human Brachyury Cell Signaling Technology Cat#94663 (1:200 dilution)
Alexa Fluor® 647 rabbit anti-human Vimentin Cell Signaling Technology Cat#9856; RRID:AB_10834530 (1:400 dilution)
Alexa Fluor® 488 mouse anti-human CD144 Invitrogen, Cat#53-1449-42; RRID:AB_10753926 (1:50 dilution)
CD31-APC Invitrogen, Cat#50-149-40; RRID:AB_657736 (1:50 dilution)
CD144-PE Miltenyi Biotec, Cat#130-135-356; RRID:AB_2751492 (1:50 dilution)
CD31-FITC Miltenyi Biotec, Cat#130-117-390; RRID:AB_2733637 (1:50 dilution)
MNX1/HB9 DSHB, Cat#81.5C10; RRID:AB_2145209 (1:10 dilution)
Alexa Fluor® 488 donkey anti-mouse IgG ThermoFisher, Cat#A-21202; RRID:AB_141607 (1:500 dilution)
CD31 R&D Systems, Cat#AF806; RRID:AB_355617 (1:200 dilution)
ZO-1 Invitrogen, Cat#33-9100; RRID:AB_2533147 (1:200 dilution)
Alexa Fluor® 647 donkey anti-sheep IgG Invitrogen, Cat#A21448; RRID:AB_2535865 (1:500 dilution)
Alexa Fluor® 488 donkey anti-mouse IgG Invitrogen, Cat#A21202; RRID:AB_141607 (1:500 dilution)

Validation

All antibodies used are commercially available with validation data for the application they were used for available on the datasheets provided for each antibody

Eukaryotic cell lines

Policy information about cell lines and Sex and Gender in Research

Cell line source(s)

Human induced pluripotent stem cells

Authentication

The parental cell line, LUMCi004-A-2, was authenticated by STR analysis (doi: 10.1016/j.scr.2022.102991) and also contains a unique targeting construct that was then used to confirm the identity of cell lines used in this study. Karyotyping by g-banding and ddPCR was performed on the cell line used in this study and is shown in Supplementary Figure 1.
The previously published LUMCi004-A-1 (LU99_AAVS1-bxb-v2) hiPSC line (doi: 10.1016/j.scr.2022.102991) was also used in this study in Supplementary Figure 2, and authenticated based on the unique targeted construct it contains. All lines used in this study are female (XX, normal).

Mycoplasma contamination

The LU99_CLYBL_bxb1_Dual (STRAIGHT-IN Dual, hPSCreg: LUMCi004-A-8) and the LU99_AAVS1-bxb-v2 (hPSCreg: LUMCi004-A-1) hiPSC lines tested negative for mycoplasma contamination using the MycoAlert® Mycoplasma Detecton Kit (Lonza,#LT07-318).

Commonly misidentified lines
(See ICLAC register)

No commonly misidentified lines were used in this study.

Plants

Seed stocks — *Report on the source of all seed stocks or other plant material used. If applicable, state the seed stock centre and catalogue number. If plant specimens were collected from the field, describe the collection location, date and sampling procedures.*

Novel plant genotypes — *Describe the methods by which all novel plant genotypes were produced. This includes those generated by transgenic approaches, gene editing, chemical/radiation-based mutagenesis and hybridization. For transgenic lines, describe the transformation method, the number of independent lines analyzed and the generation upon which experiments were performed. For gene-edited lines, describe the editor used, the endogenous sequence targeted for editing, the targeting guide RNA sequence (if applicable) and how the editor was applied.*

Authentication — *Describe any authentication procedures for each seed stock used or novel genotype generated. Describe any experiments used to assess the effect of a mutation and, where applicable, how potential secondary effects (e.g. second site T-DNA insertions, mosiacism, off-target gene editing) were examined.*

Flow Cytometry

Plots

Confirm that:

☐ The axis labels state the marker and fluorochrome used (e.g. CD4-FITC).

☒ The axis scales are clearly visible. Include numbers along axes only for bottom left plot of group (a 'group' is an analysis of identical markers).

☐ All plots are contour plots with outliers or pseudocolor plots.

☒ A numerical value for number of cells or percentage (with statistics) is provided.

Methodology

Sample preparation — The hiPSCs, hiPSC-derived neurons, hiPSC-derived endothelial cells and hiPSC-derived cardioids were dissociated to single cells using either 1x or 5x TrypLE Select at 37°C for 5 (hiPSCs, hiPSC-derived neurons and hiPSC-derived endothelial cells) or 10 (cardioids) minutes, and the cell suspension filtered using a test tubes with a cell stainer of mesh size of 35 µm. The cells were analysed live since they expressed fluorescent reporters, except for the expression of pluripotency and endothelial cell markers. In this instance, the hiPSCs were fixed and permeabilised using the FIX and PERM™ Cell Permeabilization Kit (Invitrogen) according to manufacturer's instructions. The hiPSCs were incubated with the conjugated antibodies OCT3/4-BV421, NANOG-PE and SSEA4-FITC (all BD Biosciences) for 20 minutes at room temperature and in the dark. All antibodies were diluted in permeabilization medium (medium B; Invitrogen). The cells were washed once with PBS+/+ 10% FBS and resuspended in ~300 µL of this solution. For assessment of endothelial cell markers, cells were incubated with the conjugated antibodies CD144-FITC (Invitrogen) and CD31-APC (Invitrogen), or CD144-PE (Miltenyi Biotec) and CD31-FITC (Miltenyi Biotec).

Instrument — All flow cytometric data was acquired using MacsQuant VYB (Miltenyi Biotec) or Attune™ NxT (ThermoFisher) flow cytometers.

Software — The data was analysed using FlowJo software (v. 10.2, FlowJo).

Cell population abundance — 1-1.5 x 10^4 viable (based on size) single cells were analysed for each experiment.

Gating strategy — Forward and side scatter gates were used to identify the cell population and exclude debris. Forward scatter height and area gates were used to exclude cell doublets. The boundaries between "positive" and "negative" cells or stained cells were defined based on the parental cell line or an unstained sample.

☒ Tick this box to confirm that a figure exemplifying the gating strategy is provided in the Supplementary Information.